Student thesis series INES nr 735

Simulating water temperature in Lake Vättern in Sweden using a 3D lake model

Loa Andersson

2025
Department of
Physical Geography and Ecosystem Science
Lund University
Sölvegatan 12
S-223 62 Lund
Sweden

Loa Andersson (2025).
Simulating water temperature in Lake Vättern in Sweden using a 3D lake model

Master's degree thesis, 30 credits in *GIS and Remote Sensing within the field of Geomatics*
Department of Physical Geography and Ecosystem Science, Lund University

Level: Master of Science (MSc)

Course duration: *January* 2025 until *June* 2025

Simulating water temperature in Lake Vättern in Sweden using a 3D lake model

---

Loa Andersson

Master thesis, 30 credits, in
GIS and Remote Sensing within the field of Geomatics

Supervisors:
Zheng Duan
Department of Physical Geography and Ecosystem Science,
Lund University

Daniel Palm
Department of Wildlife, Fish and Environmental Studies,
Swedish University of Agricultural Sciences

Exam committee:
Marko Scholze
Department of Physical Geography and Ecosystem Science,
Lund University

Xiaoyue Zhang
Department of Physical Geography and Ecosystem Science,
Lund University

Acknowledgment

I would like to express my deepest gratitude to my supervisor Zheng Duan for the support and guidance through this process. I also extend my sincere thanks to the Swedish University of Agricultural Sciences and the County Board of Jönköping County for providing access to essential data.

Additionally, I am truly grateful to Susanna Olsson and the entire Department of Physical Geography and Ecosystem Science for providing the study support that has been essential in completing my education.

Finally, I am profoundly grateful to my family and friends, whose support has been a constant source of strength and motivation. Their encouragement has carried me through a journey that goes beyond the scope of this master´s thesis.

Thank you.

Abstract

Lake ecosystems are increasingly affected by climate change, leading to prolonged periods of elevated water temperatures. This warming reduces surface water density, intensifying thermal stratification and trapping cold water in deeper layers. Consequently, cold-water fish and other organisms are confined to limited deep-water habitats. Understanding lake thermal structure is crucial for effective fish management and ecosystem conservation. However, the lack of in-situ temperature measurements across full depth gradients necessitates the use of three-dimensional hydro-thermodynamic models. While these models are valuable, they require reliable in-situ data for validation, presenting a significant challenge. This study simulates the three-dimensional water temperature distribution in Lake Vättern, Sweden, using the Delft3D Flexible Mesh Suite 2D3D and evaluates the model performance. Additionally, the study explores the potential and limitations of telemetry temperature data, a previously unexamined in-situ data source for hydro-thermodynamic model calibration and validation. Using telemetry data from 2023 provided by Swedish University of Agricultural Sciences (SLU), this study investigates the temperature lag in transmitter instruments, an element acknowledged as a major source of uncertainty in temperature measurements. Validation of transmitter temperatures showed promising accuracy with a one-hour depth residence threshold, though limited observations hindered statistical reliability. Consequently, only stationary telemetry receiver temperatures were used for model validation. The simulated water temperatures showed moderate accuracy, presumably due to the absence of turbulence parameter calibration. However, the most significant errors likely stemmed from validation data limitations, particularly the absence of telemetry receivers at critical depths. While challenges remain, telemetry emerges as a promising in-situ data source for lake water temperatures that justifies continued research efforts.

Table of Contents

1. Introduction

Climate change is significantly altering lake ecosystems worldwide, particularly trough rising water temperatures and decreasing ice cover duration (Magnuson et al., 2000). The fastest temperature increases have been observed in the mid- and high latitudes of the Northern Hemisphere, where several lakes are warming faster than the surrounding air (Schneider & Hook, 2010). As the temperature in the upper parts of a water body increases, the density of the water decreases. When the density contrast between the warmer surface water and the cooler, deeper water becomes sufficiently pronounced, thermal stratification develops (Boehrer & Schultze, 2008). This phenomenon is marked by the stagnation of circulation between surface and deep-water layers. The water column becomes divided into three distinct layers: the epilimnion, composed of warmer, low-density water at the surface; the hypolimnion, consisting of cooler, high-density water at the bottom; and the thermocline, a transitional zone characterized by sharp temperature gradients and minimal mixing between the upper and lower layers (Mortimer, 1952). In lakes located in the mid- and high latitudes of the Northern Hemisphere, thermal stagnation naturally occurs during the summer due to seasonal increases in surface water temperature. This stratification is typically resolved in the autumn when surface temperatures cool, allowing the water column to mix again (Boehrer & Schultze, 2008). These temperature dynamics have a significant impact on aquatic life, creating seasonal variations in the available habitat for organisms that depend on cold water < 19°C (McDonald et al., 2022). As climate warming prolongs the stratification period, fish and other aquatic organisms face escalating challenges, notably habitat loss. This loss initiates cascading ecological consequences, including disruptions to predator-prey dynamics and regime shifts (Angeler et al., 2014; Flood et al., 2021; Magnuson et al., 2000; Scheffer et al., 2003).

Given the critical ecological importance of water temperatures, accurate temperature data are essential for predicting ecological patterns and supporting aquatic ecosystem management. Water temperature data can be used to predict fish egg maturation time, identify suitable fish habitats, and delineate zones avoided or preferred by specific fish species (Régnier et al., 2017). Such information is essential for developing effective management strategies and potentially mitigating future regime shifts (Angeler et al., 2014). The demand for this type of data can also be interpreted as high given the extent of its use in scientific studies addressing the impacts of climate change on aquatic ecosystems (Whitehead et al., 2009). However, long-term and spatially comprehensive temperature observations are frequently lacking. Surface temperature data can be reliably acquired through remote sensing (ESA, 2024; NOAA, n.d.), but obtaining accurate temperature measurements throughout the water column remains challenging without extensive in-situ monitoring (Piccolroaz et al., 2024). One promising alternative is the use of fish telemetry data. Telemetry instruments surgically implanted in fish collect depth-specific temperature measurements, which, despite requiring preprocessing, can supplement sparse in-situ observations (Brownscombe et al., 2019). For instance, telemetry is currently employed in Lake Vättern, Sweden, to track migratory behaviours and habitat preferences of cold-water species such as Arctic char (*Salvelinus alpinus*) and grayling (*Thymallus thymallus*) (Swedish University of Agricultural Sciences, 2021).

In response to the temporal and spatial limitations of observed data, mathematical modelling represents a critical tool for generating continuous and spatially explicit temperature profiles in lakes (Piccolroaz et al., 2024). The simulation of water

temperatures trough mathematical modelling yields varied outputs depending on the application of the model. While the temporal and spatial coverage is determined by how the models are utilized, the models also differ in the number of dimensions they simulate and the degree of spatial autocorrelation between simulated points. Mathematical models can range from zero-dimensional surface temperature simulations and one-dimensional depth profiles to two-dimensional surface temperatures and fully three-dimensional hydro-thermodynamic simulations (Piccolroaz et al., 2024). The suitability of a model depends on its application and the availability of input data. The movement dynamics of fish varies throughout the day and across seasons. These dynamics includes the entire water body and are strongly influenced by summer stagnation. For this reason, a three-dimensional hydro-thermodynamic simulation provides the most suitable data for decision-making in management modelling highlighting the mixing characteristics of the lake and temperatures at different depths.

Mathematical models for simulating water temperatures involve a trade-off between complexity and accuracy, enabling their practical implementation (Bek et al., 2019). One widely used mathematical model is the Navier-Stokes equations (Piccolroaz et al., 2024), a set of partial differential equations that describe the motion of a fluid with constant density (Chorin, 1967). These equations can also model parameters beyond temperature, such as currents and sediment transport, and are applied in a simplified form with specific assumptions in several software packages designed for hydrological process simulations (Piccolroaz et al., 2024). One such software package is the Delft3D Flexible Mesh Suite 2D3D, developed by Deltares (2025a). Both the current and earlier versions of this software have been utilized in numerous applications, including lake temperature simulation with meteorological forcing in various regions worldwide (Amadori et al., 2021; Bermúdez et al., 2018; Cardoso-Mohedano et al., 2019; Chanudet et al., 2012; Kranenburg et al., 2020; Menten et al., 2023; Schwindt et al., 2023; Sharaf et a., 2021; Soulignac et al., 2018). The software has demonstrated mean absolute errors (MAE) ranging from 0.1°C to 1.02°C when comparing observed and simulated temperatures. However, the software's accuracy heavily depends on the availability of high-quality input, calibration and validation data. Significant differences in the spatial and temporal resolution of in-situ temperature observations across depth columns between studies further highlight the scarcity of subsurface temperature measurements in lakes.

Management of both cold-water fish and fish adapted to higher temperatures in Lake Vättern would be enhanced through the availability of temperature data with high spatial and temporal resolution in three dimensions (A. Halldén, Swedish County Board, personal communication, November 15, 2024). Such data would enable calculations of habitat volumes, fish egg maturation times, and areas avoided by certain species due to temperature preferences.

This master's thesis aims to enhance our scientific understanding of lake thermal dynamics under climate-driven warming by applying and evaluating a state-of-the-art three-dimensional hydro-thermodynamic model (Delft3D Flexible Mesh Suite) to simulate the spatiotemporal variability of water temperatures in Lake Vättern, Sweden. Additionally, this study aims to critically examine the potential of fish telemetry data as an innovative source of thermal observations for model calibration and validation, thereby addressing the widespread issue of limited in-situ data availability.

The objectives of the study are to:

- Simulate hourly three-dimensional water temperatures for the entire year of 2023 in Lake Vättern.
- Evaluate the performance of the beta version of the Delft3D Flexible Mesh Suite (hereafter referred to as Delft3D) in terms of computational efficiency, ease-of-use, accuracy, and potential for effective visualization of lake temperature dynamics.
- Assess the applicability and limitations of using fish telemetry data as input and validation for three-dimensional hydro-thermodynamic simulations, thereby broadening the sources of temperature observations for these models.

This thesis will answer the following research questions:

- How well do the simulated three-dimensional water temperatures for the year 2023 in Lake Vättern align with observed temperatures, and what factors influence the model's accuracy?
- To what extent can fish telemetry data be used as a source for the calibration and validation of hydro-thermodynamic three-dimensional simulations in the absence of other in-situ data, and what limitations need to be considered in this application?

2. Background

The following chapter provides a comprehensive overview of the theoretical background relevant to this thesis, laying the foundation for the study. Key concepts and principles that underpin the research are introduced and discussed in detail, including meteorological forcing, the theories underlying the Navier-Stokes equations, and the utilization of telemetry data. These foundational concepts are central to understanding the hydro-thermodynamic and ecological dynamics of Lake Vättern, as well as the processes that underlie the simulation conducted with Delft3D.

2.1 Simulation of lake temperatures trough Meteorological Forcing

The dynamics of water temperature in lakes can be understood through two primary processes: (1) the heating or cooling of the water surface and (2) the horizontal and vertical mixing of temperatures within the lake boundaries (SMHI, n.d.-b). Delft3D simulates these processes using meteorological input data, such as wind, heat flux, and atmospheric conditions, to model how temperature variations evolve within a three-dimensional space defined by the user (Deltares, 2025a). This section elaborates on the key drivers influencing these dynamics, explores their interactions across different stages that shape the overall thermal behaviour of lakes, and explains how Delft3D integrates these factors into its simulations to provide a comprehensive temperature model.

2.1.1 The cooling and heating of surface water

Solar radiation absorbed by the lake's surface leads to an increase in water temperature. The rate and extent of this warming depend on the intensity and duration of solar radiation, which varies across seasons. During summer, when radiation intensity and daylight duration are at their peak, the warming of surface water becomes most pronounced. The effect of surface water heating from solar radiation is also influenced by the water's visibility depth, measured using the Secchi disc (hereafter referred to as Secchi depth). A Secchi disc is a bright, circular plate that is lowered into the water until it is no longer visible, at which point the depth is recorded. When Secchi depth is shallow, often due to high concentrations of organic matter in humic water, light attenuation increases in the surface layers. This intensified attenuation traps solar energy near the surface, resulting in an enhanced heating effect in the uppermost water layers (Yang et al., 2020).

The temperature of the surrounding air is also strongly influenced by solar radiation. Solar energy heats the ground and surrounding objects, which then emit longwave radiation, transferring heat to the ambient air and raising its temperature (Schmid & Köster, 2016; Sharma et al., 2015). Heat exchange between air and water occurs through two primary mechanisms: latent heat flux and sensible heat flux. Latent heat flux is associated with evaporation, during which liquid water transitions into water vapor, removing energy from the water body and thus cooling the surface. The higher the relative humidity of the surrounding air, the less evaporation occurs, because the air is already saturated. This reduction in evaporation leads to a decrease in latent heat flux, limiting the cooling effect on the water surface. Similarly, the reverse can happen through increased wind, which lowers the relative humidity in the air and increases latent heat flux from the lake surface, or increased air pressure which decreases the latent heat flux (Venäläinen et al., 1999). Sensible heat flux occurs via convection, where heat is transferred through temperature gradients between air and water

(Bouffard & Wüest, 2019). For example, warmer air and water rises while colder, denser air and water sinks, facilitating heat movement trough heat differences between the lake surface and the ambient air.

These processes are highly influenced by cloud cover. Clouds can act as both insulators and reflectors of solar radiation. During daylight, thick clouds can block sunlight from reaching the water surface, limiting surface heating. At night, the opposite occurs, where clouds help retain longwave radiation emitted by the Earth's surface, minimising heat loss and reducing the cooling of surface water (Schmid & Köster, 2016; Sharma et al., 2015). The significance of these two effects of cloud cover depends on the extent and thickness of the cloud layer.

2.1.2 The transport and mixing of temperatures in the lake water

The movement of water temperatures through lakes occurs via several processes. The most apparent of these is molecular diffusion, a natural mechanism that works to equalize temperature gradients within the lake. However, as molecular diffusion operates at the microscopic level with short inconsistent movements in both distance and direction, it is a slow process, becoming significant only over short distances and long-time scales (Imboden & Wüest, 1995). A faster mechanism for temperature redistribution is turbulent diffusion. This process is driven by chaotic water movements, primarily caused by wind, occasional small currents, or flow over irregular bottom structures (Herb & Stefan, 2005). Additionally, wind and waves have a direct mixing effect by applying external force to the lake's surface, creating a barotropic condition with horizontal pressure. This pressure generates wind-driven internal waves that push surface water downward, redistributing heat more deeply within the water column (Flood et al., 2021; Mortimer, 1952). Because wind significantly affects temperature changes within the water body, this contributes to uneven heat distribution across the lake. Areas with greater wind exposure experience more mixing.

Convection, driven by buoyancy forces, governs the temperature exchange within the water body similarly to the exchange between the water surface and the air through baroclinic conditions. Colder, denser water sinks while warmer, less dense water rises, leading to vertical mixing and contributing to buoyancy-driven circulation within the stratified layers of the lake (Imboden & Wüest, 1995). External inputs, such as inflows, outflows, and precipitation, also affect water temperature by introducing or removing water, which in turn contributes to currents. Together, these processes create seasonal underwater currents that vary in both size and strength (Beletsky et al., 1999). The currents distribute water temperatures through a movement mechanism known as advection.

The physical form of the lake determines the extent to which hydrodynamic forces occur and whether they are significant enough to influence lake temperatures. Very shallow and small lakes are less affected by convection and seasonal currents due to insufficient density differences and depth for these processes to take place. In contrast, larger lakes retain heat longer, resulting in slower and more gradual changes in temperature dynamics. The spatial characteristics of the lake, such as its size, depth, bottom structure, shore zone morphology, and surrounding topography, are crucial in shaping how transport and mixing occur in the water column (Imboden & Wüest, 1995). In deeper lakes, seasonal thermal stratification influences the dynamics of heat transport, as mixing between thermal layers ceases (Mortimer, 1952). This restricts

advection within the respective layers, while molecular diffusion across the thermocline remains too slow to significantly alter temperatures between the layers. Wind, however, has a pronounced effect on thermocline depth, impacting the volumes of the epilimnion and hypolimnion. Higher wind speeds generate larger internal waves, causing the thermocline to oscillate and shift deeper within the water column (Flood et al., 2021).

2.1.3 Meteorological forcing in Delft3D

Fluctuations in surface water temperatures resulting from heat fluxes are calculated in Delft3D using a composite model originally designed for the Northern Ocean but also validated for large lakes. This model requires specific input parameters, including time series of relative humidity (in percentage), air temperature (in degrees Celsius), cloud cover (in percentage), solar radiation (in watts per square meter), wind speed and direction (in meters per second), and air pressure (in pascal). Based on these inputs, the model calculates effective back radiation and heat losses from evaporation and convection, accounting for enhanced evaporation driven by wind and reduced evaporation under higher atmospheric pressure. Additionally, when density gradients between air and water become significant, the model accounts for free convection, enabling further transfer of latent and sensible heat (Deltares, 2025a, Deltares, 2025b).

The output of the composite model provides temperature dynamics that are used directly in the hydrodynamic calculation but also to calculate the water density variations via an equation of state. These density variations give rise to baroclinic pressure gradients that drive flow and is used in the hydrodynamic calculation. Wind and air pressure are used to calculate barotropic gradients as input to the hydrodynamic calculation but also directly as these processes force flow by themselves. For the vertical turbulent viscosity and diffusivity in tree-dimensional simulation, closure models based on the eddy viscosity concept are used. The hydrodynamic calculation is done by solving the Navier Stokes equations for an incompressible fluid, under the shallow water and the Boussinesq assumptions (Deltares, 2025a, Deltares 2025b).

The Navier-Stokes equations are inherently complex and require simplifications to be effectively applied in hydrodynamic modelling (Steinmoeller, 2014). The shallow water assumption considers the horizontal dimensions to be much larger than the vertical (depth), allowing vertical accelerations to be neglected in the vertical momentum equation. This leads to the hydrostatic pressure approximation, simplifying the calculations of vertical forces. At the same time, the continuity equation ensures mass conservation within the system, meaning that vertical velocities are still determined based on horizontal flow variations, even though vertical accelerations are excluded. The Boussinesq assumption treats water density as nearly constant in the equations of motion, except when accounting for density variations that contribute to pressure gradients (baroclinic effects). Together, these assumptions simplify the Navier-Stokes equations into a system of partial differential equations that describe horizontal motions (via momentum equations) and vertical motion (through the continuity equation, maintaining overall mass balance).

The three-dimensional momentum equations in the horizontal (x and y directions) are given by Equations 1 and 2 (Deltares, 2025a; Soulignac et al., 2018).

$$\frac{\partial u}{\partial t} + u\frac{\partial u}{\partial x} + v\frac{\partial u}{\partial y} + w\frac{\partial u}{\partial z} - fv = -\frac{1}{\rho 0}\frac{\partial P}{\partial x} + F_x + \frac{\partial}{\partial z}\left(\vartheta_E \frac{\partial u}{\partial z}\right) + M_x$$

Equation 1

$$\frac{\partial v}{\partial t} + u\frac{\partial v}{\partial x} + v\frac{\partial v}{\partial y} + w\frac{\partial v}{\partial z} - fu = -\frac{1}{\rho 0}\frac{\partial P}{\partial y} + F_y + \frac{\partial}{\partial z}\left(\vartheta_E \frac{\partial v}{\partial z}\right) + M_y$$

Equation 2

The three-dimensional continuity equation in the vertical (z-direction) is given by Equation 3 (Deltares, 2025a).

$$\frac{\partial h}{\partial t} + u\frac{\partial uh}{\partial x} + v\frac{\partial vh}{\partial y} + \frac{\partial w}{\partial z} = h(q_{in} - q_{out})$$

Equation 3

Where x, y and z are Cartesian coordinates (m), describing the spatial dimensions. t is time (s). u, v, and w are the three components of the water velocity (m/s). f is the Coriolis frequency in 1/s, accounting for the rotational effects of the Earth. $\rho 0$ is the water density (kg/m3), treated as constant according to the Boussinesq assumption. P is the pressure (Pa), which includes barotropic and baroclinic effects. ϑ_E is the vertical eddy viscosity coefficient, describing the turbulent vertical momentum transfer. F is the forces contribution to turbulent, such as wind. M are contributions from external sources, such as inflows/outflows. h is the water depth (m), and q is the amount of water flowing in and out trough participation, tributary and evaporation.

Several hyperparameters, unique to each lake, must be determined and specified for Delft3D to solve these equations with high accuracy. The input data and hyperparameters used are presented in the methodology part of this report.

2.2 Potential and challenges of telemetry technology

As previously mentioned, transmitters are surgically implanted into the abdominal cavities of fish for monitoring purposes (see Figure 1), with the procedure being performed while the fish is anaesthetized. These transmitters emit acoustic signals that are detected by stationary receivers, strategically placed near the lakebed to maximize coverage within their detection radius (Thorstad et al., 2013). The transmitted acoustic signals encode a range of information, including fish species, individual identification codes, and swimming speeds. Additionally, the signals can include temperature and pressure data, which can be further processed to infer the fish's depth within the water column (Rogers & White, 2007). However, the accuracy of this data is subject to significant limitations (Brownscombe et al., 2019). Firstly, it is not possible to determine the precise spatial location of a fish relative to its transmitter at the time of data collection, as receivers operate within detection zones whose ranges vary depending on the technology utilized (see Figure 1). Secondly, fish exhibit vertical movement, and when transitioning between water layers or locations, the temperature recorded by the transmitter within the abdominal cavity does not immediately equilibrate with the surrounding water, as the abdominal walls act as an insulator. This thermal lag may introduce temporal discrepancies and result in inaccurate temperature readings associated with the detected depth, since depth measurements based on pressure respond instantaneously to fish movement, whereas changes in abdominal

temperature occur with a delay. A previous study applied a residence time threshold of 20 minutes for a ±1-meters depth range to ensure the reliability of temperature measurements inside the fish abdominal (Kristensen et al., 2018). However, the study describes an observation of temperature lag when fish changes depths but did not present validation for the threshold used.

Furthermore, depth and temperature are not recorded simultaneously but rather at variable intervals (see Figure 1), which adds to uncertainty in the temperature data. Despite these errors, the high update frequency of telemetry detections, unique to each dataset, generally leads to the generation of large datasets, even after extensive filtering to ensure the validity of data for analysis (Brownscombe et al., 2019).

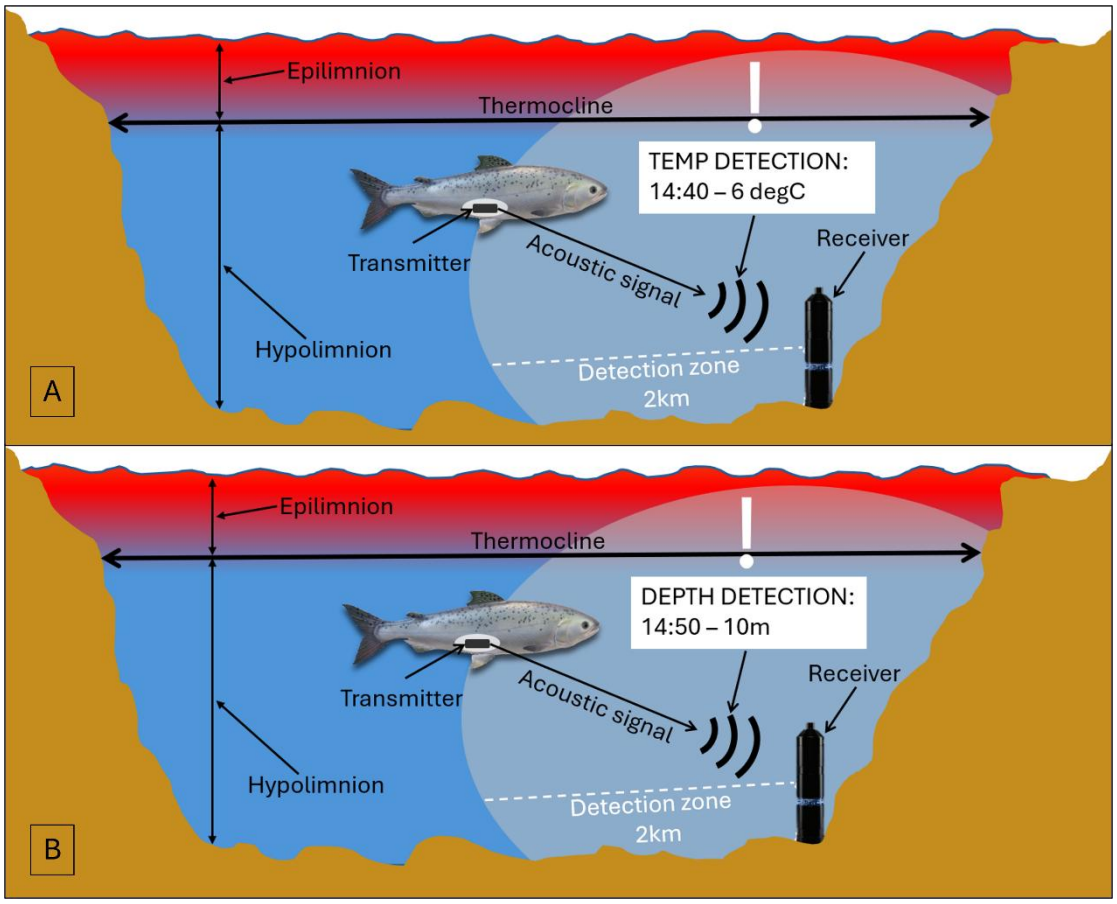

Figure 1: The usage of telemetry temperatures was investigated during a Master´s thesis study. Images A and B illustrate both the distinct temperature layers during summer stratification and the practical application of telemetry data. The key difference between the two images is the type of detection: Image A displays a temperature detection at 14:40, whereas Image B shows a depth detection at 14:50. This highlights the non-simultaneous recording of depth and temperature, which must be addressed during data processing, as fish may move between stratification layers within minutes. Consequently, temperature readings paired with a delayed depth detection may not accurately reflect the thermal conditions at the fish's actual position.

3. Data and methodology

The methodology of this study can be divided into five parts. The description of the study area, the validation of temperature measurements from telemetry data, the simulation of water temperatures in Delft3D, the calibration and validation of the three-dimensional model and data compatibility. This section will describe all the data retrieved for the study and each part of the method in chronological order.

3.1 Study area

Lake Vättern is Sweden's second-largest lake, extending 135 kilometres from south to north, with a maximum width of 31 kilometres. The lake reaches a maximum depth of 120 meters and spans a surface area of 6,376 square kilometres. Formed by a fault in the Earth's crust, its elongated shape and significant depth are notable features (see Figure 2). The lake's water level, approximately 88.5 meters above sea level, fluctuates by only around 30 cm throughout the year (SMHI, n.d.-a). Lake Vättern is nutrient-poor, resulting in exceptionally clear water with a Secchi depth of 10–15 meters, depending on the season and measurement location (Vätternvårdsförbundet, n.d.). The northern parts of the lake are characterized by a hilly bottom structure and archipelago-like groups of islands. The shoreline includes abundant reeds, vegetation, rocks, and stones. In contrast, the southern parts of the lake are more uniform, featuring steep rocky edges, minimal aquatic vegetation, and no island groups. The largest island, Visingsö, covers an area of 2,504 hectares (SCB, 2008).

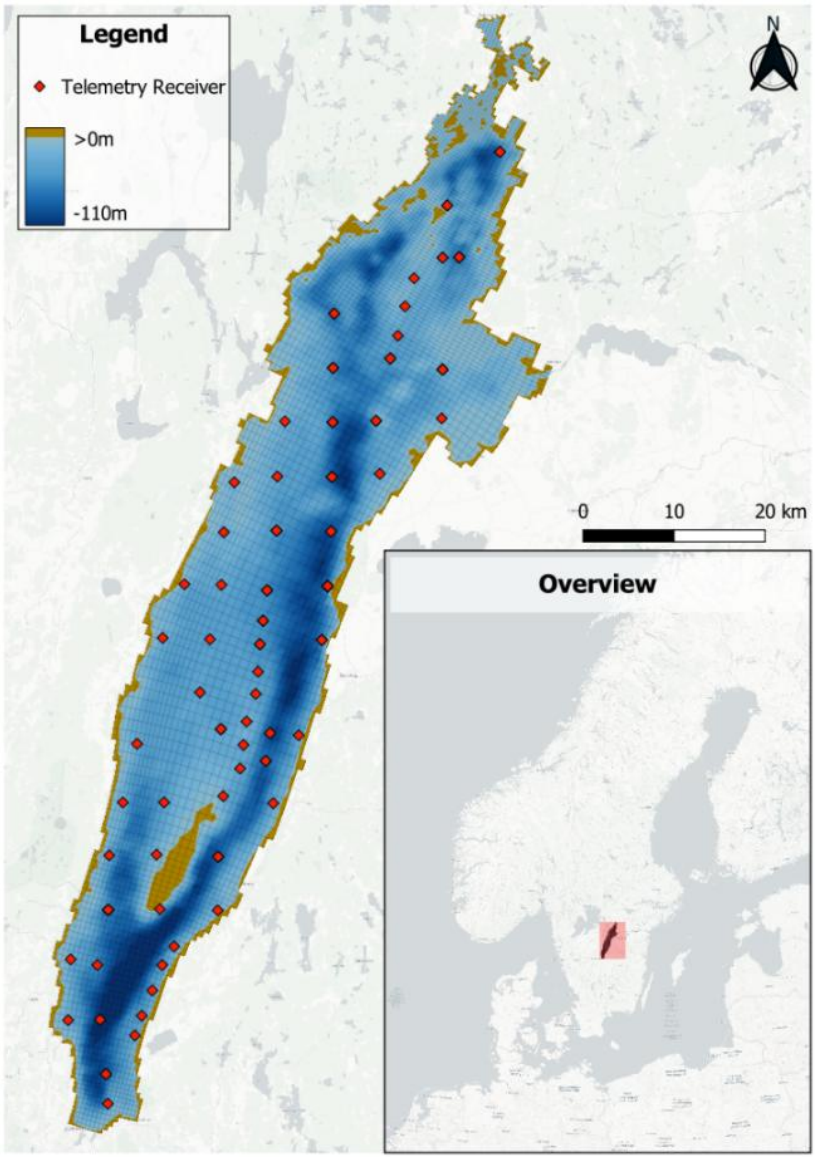

Figure 2: Figure 2 illustrates key spatial data used to validate the hydrodynamic model and visualizes the three-dimensional characteristics of Lake Vättern, Sweden. The blue gradient represents lake depth, while brown regions depict land surfaces. The red dots show the 2023 locations of telemetry receivers, which were processed and used as input and ground truth data during the setup and validation of a Delft3D Flexible Mesh Suite 2D3D model. Both depth and telemetry data was provided by Swedish University of Agricultural Sciences (SLU). Background: Carto Light ©CartoDB.

3.2 Data

Bathymetry data, provided in shapefile format, was obtained from Swedish University of Agricultural Sciences (SLU), with 10-meter depth isolines. Additionally, hydrology data in shapefile format (land boundary) and raster representations of digital elevation models (DEM) were retrieved from SLU's geodata catalogue (Swedish University of Agricultural Sciences, n.d.). Telemetry data was obtained from SLU, with the year 2023 selected due to its completeness in both depth and temperature measurements. A total of 506,507 transmitter observations were recorded, distributed across 57 receivers. The spatial distribution of the receivers is illustrated in Figure 2. All data and corresponding licensing are presented in Table 1.

Table 1: Overview of the datasets used in the three-dimensional water temperature simulation of Lake Vättern, Sweden. The simulation was performed using a Delft3D Flexible Mesh Suite FM 2D3D model with meteorological forcing. Special licensing for the bathymetry and telemetry data was exclusively granted for the study by the Swedish University of Agricultural Sciences (SLU). Details on the telemetry data is found in Table 2. Details on the meteorological data (ERA5-Land/Single level) is found in Table 3.

Data	Description/Usage	Format/ Resolution	Provider	License
Bathymetry	Used to create elevation model together with DEM	**Format:** Shapefile **Spatial resolution:** 10m	SLU	Special
DEM	Used to create elevation model with lake depths	**Format:** Raster **Spatial resolution:** 2m	Swedish Land Survey	CC0
Lake boundary	Used to create a land boundary file of lake Vättern	**Format:** Shapefile **Spatial resolution:** -	Swedish Land Survey	CC0
Telemetry data	Used to extract temperature measurements throughout the water column	**Format:** RData **Spatial resolution:** 2km **Temporal resolution:** Minute interval throughout 2023	SLU	Special
Meteorological data	Used for the meteorological forcing	**Format:** NETCDF4 **Spatial resolution:** see Table 3 **Temporal resolution:** Hourly	European Centre for Medium-Range Weather Forecasts	CC0

The telemetry data consisted of two instrument categories: transmitters and receivers (see Table 2). The transmitter, which was implanted in the abdominal cavity of the fish, was an Innovasea V9TP-2x-BLU-1 or VT13TP-1x-BLU-1-0136M. These devices had a thermal resolution of 0.15°C and a depth resolution ranging from 0.075 m to 0.6m within the depth range of 17–136m. The accuracies were ±0.5°C for temperature measurements and between ±0.5m and ±6.8m for depth measurements within the same depth range (see Table 2). The receiver was of the type Innovasea VR2AR and VR2Tx, both of which utilized the same sensor. This sensor featured a thermal resolution of 0.1°C and an accuracy of ±0.5°C.

Table 2: Overview of the telemetry instruments used to record depth and temperature data from Lake Vättern, Sweden, during 2023. The data was collected by Swedish University of Agricultural Sciences (SLU) and utilized in a master's thesis at Lund University to validate the Delft3D Flexible Mesh Suite model.

Instrument	Thermal resolution	Thermal accuracy	Depth resolution (Depth 17-136m)	Depth accuracy (Depth 17-136m)
Receiver: VR2AR/VR2Tx	0.1°C	±0.5°C	-	-
Transmitter: V9TP-2x-BLU-1	0.15°C	±0.5°C	0.075m (at 17m) 0.6m (at 136m)	±0.5m (at 17m) ±1m (at 136m)
Transmitter: VT13TP-1x-BLU-1-0136M	0.15°C	±0.5°C	0.075m (at 17m) 0.6m (at 136m)	±1.7m (at 17m) ±6.8m (at 136m)

ERA5-Land hourly data (Muñoz, 2019), and ERA5 Hourly data on single-level (Hersbach et al., 2023), for 2023 were downloaded from Copernicus Climate Change Service (2023), in NETCDF4 format organized by month. A sub-region extraction was performed when downloading the data using the following coordinates: North 59.0, West 14.0, East 15.5, and South 57.7. The variables retrieved are detailed in Table 3.

Table 3: Description of the data used for meteorological forcing in a Delft3D Flexible Mesh Suite FM 2D3D model. Note that total cloud coverage has a lower resolution compared to the other variables, as it is only available at the single-data level, which inherently has a lower resolution.

Variable	Description	Unit	Grid Resolution (°lat / °long)
2m dewpoint temp	Dewpoint temperature 2m above surface	Kelvin	0.1°
2m temperature	Temperature 2m above surface	Kelvin	0.1°
Surface solar radiation downwards	Refers to the total amount of solar energy, including direct sunlight and diffuse radiation, reaching the Earth's surface	J m^{-2}	0.1°
10m u-component of wind	The wind velocity x-component	m/s	0.1°
10m v-component of wind	The wind velocity y-component	m/s	0.1°
Surface pressure	The atmospheric pressure exerted at the Earth's surface	Pa	0.1°
Total cloud coverage	The fraction of the sky covered by clouds at the Earth's surface	Fraction ranging from 0-1	0.28125°

The software and hardware used during the study are presented in Table 4.

Table 4: Specifications of the hardware and software used in a master's thesis at Lund University, detailing their respective roles in data processing and simulation. The Delft3D Flexible Mesh Suite 2D3D model was utilized for hydrodynamic simulations, while QGIS and ArcGIS supported pre-processing tasks. Python was employed for NETCDF4 data conversion, and the system configuration ensured optimal computational performance.

Hardware/Software	Specification/Usage	Version
Lenovo Legion 5	Intel i9 24 cores; NVIDIA Geoforce RTX 4080 12gb; RAM 32gb; Windows 11	2023 years model
Delft3D Flexible Mesh Suite 2D3D	Simulation software	Beta version intended for release 2027
QGIS	General pre-processing	Desktop 3.30.3
ArcGIS	Bathymetry and DEM pre-processing	2.7.3
Python	NETCDF4 conversion	3.13.2
R	Pre-processing and statistical analysis of telemetry and meteorological data	4.4.2

3.2.1 Pre-processing of meteorological data

Relative humidity was calculated using Equation 4. Junzeng et al. (2012) describe three distinct formulas for determining saturation vapor pressure. For this study, the Magnus saturation vapor pressure formula was selected for both temperatures above and below 0°C (Equations 5 and 6), as it is particularly suited for conditions where temperatures may drop below freezing, such as the surrounding of Lake Vättern. Additionally, Upreti & Ohja (2017) propose that actual vapor pressure can be derived using the dewpoint temperature corresponding to the air temperature at the same four-dimensional spatial location, aligning with the ERA5-Land dataset. For this purpose, Tetens' formula (Equation 7) was applied. Tetens' formula provides a widely used method for estimating actual vapor pressure based on dewpoint temperature. It is commonly applied in meteorology and climatology due to its proven accuracy in describing water vapor behaviour in the atmosphere (Upreti & Ohja 2017).

$$Relative\ Humidity = \left(\frac{Actual\ Vapor\ Pressure}{Saturation\ Vapor\ Pressure}\right) \times 100$$

Equation 4

For temperatures greater than zero ($T > 0$), the saturation vapor pressure is defined by Equation 5. Similarly, for temperatures lower than zero ($T < 0$), the saturation vapor pressure is defined by Equation 6.

$$Saturation\ Vapor\ Pressure = 6.11 \times 10^{\frac{7.45 \times T}{237.3+T}}$$

Equation 5

$$Saturation\ Vapor\ Pressure = 6.11 \times 10^{\frac{9.5 \times T}{265.5+T}}$$

Equation 6

$$Actual\ Vapor\ Pressure = 6.108 \times \exp\left(\frac{17.27 \times T_{dew}}{237.3 + T_{dew}}\right)$$

Equation 7

Where T represents temperature in degrees Celsius and T_{dew} denotes the dewpoint temperature corresponding to the air temperature.

Delft3D requires surface solar radiation downward in watts per square meter (W/m²). This variable was converted from joules per square meter (J/m²) using ERA5-Land accumulation principles. ERA5-Land provides solar radiation values as cumulative energy flux, meaning each hourly value includes the accumulated radiation from previous hours (European Centre for Medium-Range Weather Forecasts, n.d.). To accurately represent instantaneous flux, the conversion incorporates the accumulated value from the previous hour, refining the calculation accordingly. During the first hour after midnight, the variable is computed using Equation 8, while for all subsequent hours, Equation 9 is applied.

$$SSR\ [Wm^{-2}] = \frac{SSR_h\ [Jm^{-2}]}{3600\ [s]}$$

Equation 8

$$SSR\ [Wm^{-2}] = \frac{SSR_h\ [Jm^{-2}]\ -\ SSR_{h-1}\ [Jm^{-2}]}{3600\ [s]}$$

Equation 9

The variable SSR_h represents the instantaneous solar radiation flux at hour h, while SSR_{h-1} denotes the accumulated radiation from the previous hour. ERA5-Land hourly data provides accumulated values over a one-hour period. Consequently, the values must be divided by 3600 seconds. This adjustment accounts for the fact that 1 watt equals 1 joule per second, ensuring the correct conversion, as described by European Centre for Medium-Range Weather Forecasts (n.d.).

The air temperature and 2m dewpoint temperature was converted from Kelvin to degrees Celsius. Total cloud coverage was transformed into a percentage by multiplying the values by 100. Uniform meteorological conditions were assumed across the entire lake area, and the hourly mean values of each meteorological variable were calculated within the lake extent (land boundary file). Details on the processing of the land boundary file are provided in section 3.4 of the methodology. Finally, the hourly time series data were exported as a CSV file and incorporated into the model setup.

3.3 Temperature measurements from telemetry data

To construct a reliable dataset of temperature measurements, it was essential to address the challenges identified by Brownscombe et al. (2019) (see Section 2.2). Since no standardized methodology for processing telemetry data was available in existing

literature, this section provides a detailed explanation of the approach taken, along with justifications for each step.

3.3.1 Overview of the telemetry processing method

The telemetry data was provided in two separate files: one containing transmitter data and the other containing receiver data. Both files shared the receiver ID as a common key, representing the receiver that detected the fish transmitter. This key played a central role in merging and filtering the dataset.

The depth and temperature readings in the transmitter dataset were recorded at different timestamps, causing temporal misalignment between depths and temperatures. As a result, appropriate temporal pairing was necessary, since a temperature reading and a depth reading taken with a significant time gap could not reliably represent each other due to temporal, horizontal and vertical variation of temperatures. To ensure accurate processing while minimizing errors, three critical knowledge gaps had to be analysed and determined from the dataset:

1. **Residence time threshold at a new depth** – This threshold was necessary to determine the point at which temperature lag within the fish's abdominal cavity had stabilized, ensuring that the recorded temperature accurately represented the new depth.
2. **Time interval for depth timestamps pairing within a residence time chain** – This interval accounted for potential undetected vertical movement between timestamps, ensuring that temperature readings at the residence time threshold were not influenced by unnoticed transient depth changes.
3. **Time interval for pairing depth and temperature timestamps** – Since depth and temperature were recorded asynchronously, this threshold was required to ensure that temperature measurements accurately represented the depth at the time of registration.

A methodological paradox arose due to these knowledge gaps: depth and temperature measurements needed to be paired to determine appropriate time intervals, but without predefined intervals, it was difficult to identify which pairs were representative. To resolve this, an experimental approach was employed, where initially arbitrary time intervals were applied. The goal was to analyse how temperature and depth fluctuated over time and to identify threshold values where variations could be considered negligible. Once these thresholds were established, the timestamp intervals were refined, and the data was re-processed to ensure that depth-temperature pairing was as representative as possible.

3.3.2 Creation of continuous time chains of depth records

An initial data cleaning process was performed to remove outliers and NA- values from both the receiver and transmitter datasets, eliminating errors and ensuring data quality. In the receiver dataset, tilt and depth measurements were reviewed, and entries with tilt angles of the receiver instrument exceeding 50 degrees and depths shallower than 9 meters were excluded. According to the data provider (F. Halldén, personal communication, January 19, 2025), such anomalies indicated that the receivers were not stationary but instead in motion, likely due to fieldwork or other external influences affecting the instruments. These non-stationary measurements were considered

unreliable, as they may have been collected outside the three-dimensional extent of the lake and were therefore removed.

Kristensen et al. (2018) used a ±1-meter depth interval for a fish to be considered residing at the same depth. This study adopted the same interval to create a basis for discussion regarding the residence time threshold used by Kristensen et al. (2018) and the threshold resulting from the analysis conducted in this study. The term "fixed depth" is therefore used in this thesis to refer to a depth interval of ±1 meter around a residence depth.

To determine whether a fish remained at a fixed depth for a given duration, continuous time chains of depth records needed to be established, ensuring that depth records were not temporally disjointed beyond a defined timestamp threshold. This threshold needed to be sufficiently small to ensure that temporary vertical movements of the fish within the time chain did not influence the transmitter temperature. However, the impact of vertical movement on temperature could only be evaluated after analysing the pairing interval for depths and temperatures or the temperature lag within the fish's abdominal cavity during movement, creating a methodological paradox where one depended on the other. To address this, an initial arbitrary pairing interval of 10 minutes was applied, ensuring that two consecutive depth records were not temporally separated by more than 10 minutes and shared the same fixed depth, animal ID, and receiver ID.

A new column was created in the transmitter dataset, assigning a unique ID to observations within the same continuous time chain of depth records. This unique ID enabled the analysis of temperature flux over time for a fish residing at a fixed depth, which was crucial for determining the appropriate time interval for pairing representative temperature measurements with depth records.

3.3.3 Pairing depth and temperature by timestamp interval

The same arbitrary 10-minute pairing interval was applied to link depth and temperature detections. Due to the fragmented nature of the detections and the absence of a continuous data stream, pairings were conducted both forwards and backwards in time, effectively resulting in a ±10-minute interval. To assess temperature variation over time at a fixed depth, changes in standard deviation (SD) were analyzed over a 15-minute period for all paired detections at fixed depths. SD was chosen for its statistical sensitivity to fluctuations in temperature and was calculated according to Equation 12. As the pairing window merely defined the outer temporal bounds, most depth and temperature detections were paired within narrower intervals. To determine the number of transmitter records (see Figure 3), data were filtered based on the observed temperature/depth pairing intervals, specifically 0-1 min, 1-5 min, 5-10 min, and 10-15 min, and the number of pairings within each interval was counted. This approach enabled a more nuanced understanding of the pairing distribution while optimizing the retention of valid detections.

The analysis revealed that SD increased significantly between 10 and 15 minutes, with a spread of approximately 0.25°C around the mean temperature, while the number of observations within this interval was low (see Figure 3). In contrast, between 5 and 10 minutes, the increase in SD was less pronounced, staying below 0.05°C. Additionally, the number of observations within this range was substantial, making it important to retain to preserve the dataset’s temporal continuity. Based on these findings, a ±5-

minute pairing interval for depth and temperature measurements was decided. This interval was shown to have minimal impact on the accuracy of telemetry temperature data while maintaining an adequate number of observations. Furthermore, the initially arbitrary 10-minute pairing interval used to establish continuous time chains of depth records was validated by this analysis, ensuring that temperature measurements at the residence time threshold remained unaffected by undetected transient depth changes.

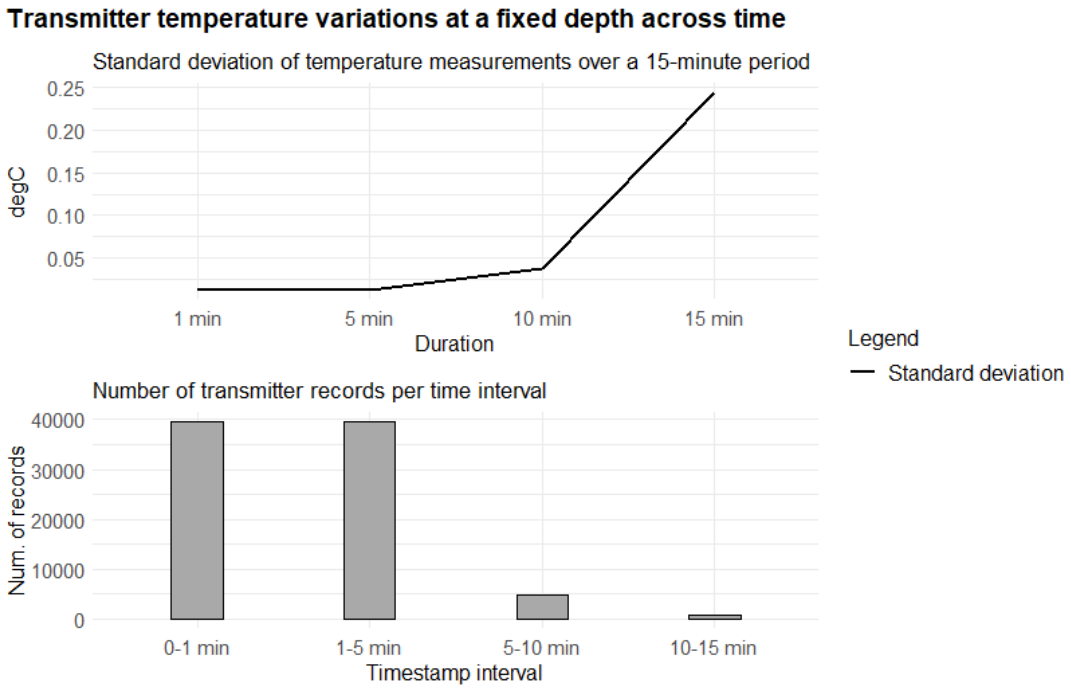

Figure 3: Variations in transmitter temperature at a fixed depth (±1 meter around the fish residence depth) were analysed. The investigation aimed to determine how long a transmitter remains at a stable depth before temperature fluctuations occur in the dataset. As indicated by the standard deviation of all transmitter temperatures recorded at the fixed depth, the temperature remains stable for the first 10 minutes, followed by a sharp increase in variability between 10 and 15 minutes. However, the amount of data available during this time interval was limited.

3.3.4 Threshold to address lag in temperature measurements

After pairing depth and temperature data and establishing continuous chains of depth records with the appropriate time interval, instances of fish shifting between depths were identified. For these cases, maintaining continuity in measurements without gaps was essential when a fish moved vertically. Only one such individual was detected (animal ID: Char_1395039). The relationship between depth changes and temperature fluctuations during the fish vertical movement was analysed by plotting the two variables (see Figure 4). When temperature changes stabilized at a new depth, the elapsed time from the first detection at that depth was recorded. The analysis revealed a temperature lag in the transmitter measurements following vertical movement, which was approximately one hour.

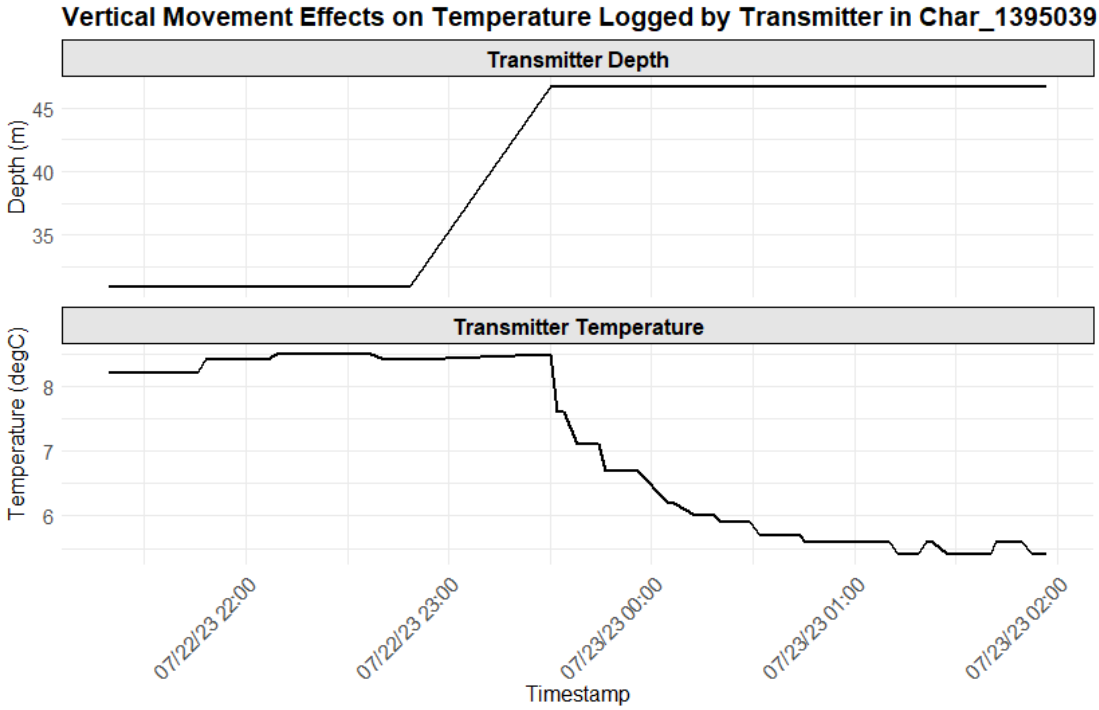

Figure 4: Depth changes and associated temperature fluctuations in telemetry data recorded for an individual fish exhibiting vertical movement were analysed. The plot illustrates the relationship between depth shifts and the corresponding temperature lag in transmitter measurements. The elapsed time from the first detection at a new depth until temperature stabilization was recorded, revealing an approximate lag of one hour.

A final processing step was conducted from the start using the validated intervals and thresholds, determined through the methodological analysis. The ±5-minute interval ensures that temperature variations remain negligible when pairing depth and temperature measurements. The 10-minute window used to create continuous chains of depth records at fixed depths prevents rapid, temporary depth changes outside the fixed depth from influencing temperature. Similarly, the one-hour residence threshold confirms that a fish has remained at a fixed depth long enough for the recorded temperature to be accurately representative.

3.3.5 Validation of transmitter temperatures

To evaluate the accuracy of transmitter temperature measurements, they were compared to receiver temperatures, which served as the ground truth. The receiver ID functioned as a common key, enabling the pairing of transmitter and receiver temperatures within a ±5-minute interval, as referenced in Figure 3. Since receiver temperatures were updated at fixed hourly intervals, most transmitter temperature timestamps fell outside the ±5-minute pairing window due to their random temporal distribution. The pairing process resulted in a total of 260 matched receiver-transmitter temperature pairs out of 150 000 possible.

Using this dataset, key statistical metrics were calculated, including Root Mean Square Error (RMSE; see Equation 13), Mean Absolute Error (MAE; see Equation 14), residual mean and SD (see Equation 12). Additionally, minimum- and maximum residual value was noted. These measures provided insights into the deviations between transmitter and receiver temperatures.

To further investigate how residence time at a specific depth affects accuracy and relate it to the threshold used by Kristensen et al. (2018), two different time thresholds, twenty minutes and ninety minutes, were tested against receiver temperatures. The aim was to further nuance whether the twenty-minute threshold used by Kristensen et al. (2018) was too short, as suggested by Figure 4, and to examine how the one-hour threshold applied in this study compares to a longer residence duration.

Given that the receiver temperature sensor had an accuracy of ±0.5°C and the transmitter sensor exhibited a similar error margin of ±0.5°C, the total uncertainty was estimated using error propagation (Equation 10). The standard deviation method was employed to account for all potential interactions between individual errors, ensuring precise assessment of overall instrument accuracy when paired in calculations (Fantner, 2013). This approach was not applied to depth measurements, as receiver depths were manually determined when deployed on the lake bottom. In these cases, depth uncertainty was solely inherited from the transmitter error of ±0.5m to ±6.8 m depending on depth (see Table 2). Furthermore, no specific data exists regarding the potential placement error of the receivers during manual deployment, which introduces an additional but unquantified source of uncertainty in depth measurements. The thermal error propagation analysis was not incorporated into the validation metric calculations but rather served as supplementary information to define the uncertainty range and refine the discussion on telemetry temperature processing accuracy.

$$Residual\ uncertainty\ = \sqrt{(\Delta x)^2 + (\Delta y)^2}$$

Equation 10

Where Δx and Δy represents the uncertainty in individual measurements.

3.3.6 Compatibility in Delft3D Flexible Mesh Suite 2D3D

The goal of telemetry processing was to generate reliable temperature measurements throughout the depth column for the entirety of 2023, which would then be used as ground truth data for the Delft3D model validation. A key challenge encountered was the compatibility between the bathymetry data used in the simulation and the depth of the temperature measurements obtained from telemetry. On occasion, the telemetry transmitters recorded depths exceeding the actual depth of the receiver. This discrepancy is expected due to the transmitters' detection range of up to 2 km, the depth variation inside the detection range and because the transmitter uses the receiver coordinates for detection. In the bathymetry file, such records were positioned beyond the maximum depth of the lake and therefore fell outside its three-dimensional extent.
To resolve this issue, the depths of the temperature measurements in the telemetry data were tested against the corresponding raster cell values in the bathymetry data. If a temperature measurement depth exceeded the bathymetry depth, the record was excluded from the dataset.

3.4 Simulation of temperatures in Delft3D

The land boundary file was derived by extracting the polygon for Lake Vättern from the hydrology data provided by the Swedish Land Survey. To create the bathymetry file, depth data in shapefile format was rasterized using ArcGIS Pro. The water surface of Lake Vättern was located at an elevation of 89m at the time of DEM creation. Since the reference plane (water surface) of the depth data was zero, the grid was subtracted by 89m. The extent of Lake Vättern in the DEM was set to zero, and the rasterized

depth data was integrated into the DEM to create a continuous bathymetry representation. Finally, the bathymetry file was clipped to the land boundary file and exported as an XYZ file.

3.4.1 Creation of irregular computation grid

A cartesian irregular grid was created using the Delft3D module RGFGRID. Land boundary file was imported, and three splines were drawn to connect the northern and southern ends of Lake Vättern. Subsequently, 20 perpendicular splines were added across the three splines. The grid was then grown from the splines to form a regular grid structure. Polygons were delineated outside the land boundary file to exclude cells that lacked overlap with the interior of the land boundary. The grid was transformed from a regular to an irregular structure, resulting in variable spatial resolution across the domain, as required by the Delft3D software (Deltares, 2025a), and refined to achieve a cell size ranging from 200m to 900m. Larger cell sizes were applied in the central part of the lake, while smaller cells were utilized closer to the shoreline to enhance the representation of nearshore dynamics while minimizing data volume. The chosen grid spacing was considered appropriate to generate a highly detailed output while ensuring computational efficiency, making the calculations feasible. According to Deltares (2025c), the orthogonality of a computational grid must remain below 0.02. This requirement was initially not met for the irregular grid; therefore, cell boundaries were manually adjusted, followed by an iterative orthogonalization function, until the grid fully complied with the orthogonality criteria.

3.4.2 Model setup

The model setup in Delft3D GUI covered a simulation period from January 1, 2023, at 00:00:00 to December 31, 2023, at 23:00:00. The bathymetry file in XYZ format was interpolated onto the irregular computational grid, applying an average interpolation for each cell. The two-dimensional grid was extended into a three-dimensional grid with a total of 60 Z-layers. Layer 1 to 30 were set to a vertical resolution of 1 meter. For layers 30 and deeper, a Sigma growth factor of 1.02 was applied, with reference to Soulignac et al. (2018) to ensure balance between vertical resolution and computational efficiency. The Sigma growth factor regulates the variation in layer thickness, increasing with depth to optimize data storage while preserving the ability to capture temperature dynamics. This approach ensures detailed representation of thermal variations from the surface to the thermocline, where temperature fluctuations are expected to be more pronounced compared to deeper water layers.

Model parameter selection was guided by the sensitivity analysis conducted by Chanudet et al. (2012), which identified the parameters exerting the greatest influence on simulation outcomes. To enhance the accuracy of parameter selection, reference was made to the study by Amadori et al. (2021), who developed a Delft3D model for a lake exhibiting similar characteristics to Lake Vättern, such as shape, orientation and depth. Their research investigated a range of calibratable parameters, many of which had been highlighted by Chanudet et al. (2012) in their sensitivity analysis. Given the similarities in physical characteristics between the reference lake and Lake Vättern, identical values were applied for the calibratable parameters with substantial impact on model results. A comprehensive overview of the model settings and parameter values is provided in Table S1 (see Appendix 1).

Due to a bug in Delft3D that prevented the correct processing of spatially varying grid data for wind components and air pressure, it was not possible to utilize spatially resolved meteorological inputs. Consequently, spatially uniform hourly data had to be applied across the entire lake for all atmospheric variables throughout the full simulation period, including cloud cover, air temperature, relative humidity, solar radiation, wind (x and y components), and air pressure. All variables were imported using the Delft3D GUI wizard. Observation points were strategically placed at each telemetry receiver location to store model outputs for validation purposes with the telemetry temperature data after the simulation. The Delft3D version used in this study did not support the transfer of attribute data from the input shapefile to the output. The observation points were therefore formatted in XYN to ensure that the output retained the input receiver ID, thereby facilitating the pairing of telemetry and simulated temperatures during validation.

When the simulation was executed within the Delft3D GUI, the output exhibited several errors, including interruptions and spatial fragmentation. To address these issues, the model was exported to a DIMR configuration file and executed via a batch script within the installation directory. OpenMP (2023) was installed and integrated into the batch script to leverage multi-core processing capabilities, utilizing available CPU cores to minimize computational time as much as possible. However, due to a misinterpretation in the implementation of OpenMP, only half of the available cores were utilized during the simulation (12 out of 24). The complete simulation runed for 12 hours and 6 minutes before coming to a normal end.

3.4.3 Model validation

The simulation output was stored in two NetCDF files. One contained hourly three-dimensional domain data, while the other stored hourly one-dimensional vertical data at observation points for validation. The complete simulation output was analysed using Delft3D's MATLAB-based tool, QUICKPLOT, to identify potential errors in the spatial representation of the results (Deltares, 2025a). To validate the numerical stability of the model, the CFL criterion was tested, which for this model setting requires a CFL < 0.6 as this was set as the maximum for the model (Deltares, 2025b). CFL was calculated using Equation 11 (SimScale, 2024).

$$CFL = \frac{U_{max} \times \Delta t}{\Delta x}$$

Equation 11

Where U_{max} is the maximum simulated flow velocity, Δt is the computational timestep and Δx is the minimum grid cell size.

The observation point output was first converted from NetCDF to CSV using Python and subsequently imported into R for validation. A join between observation points data and processed telemetry data was performed based on telemetry receiver ID and a depth interval of 1m to ensure correct pairing of receiver placements with simulation data. 1m was used as this was the vertical resolution for the simulation at the observation points. The dataset was then filtered based on temporal alignment between receiver temperature measurements and simulation output temperatures. A join threshold of ±5-minutes was applied, based on the conclusion made during telemetry temperature validation that water temperatures exhibit no significant changes within

this time frame, thereby allowing measurement and simulated temperature 10 minutes apart to be considered comparable.

In Williams & Esteves (2017), a methodological framework for validating hydrodynamic models is presented. They recommend using RMSE to assess model accuracy, defined as the difference between measured and simulated data (see Equation 13). MAE also provides an estimate of model accuracy (see Equation 14). Although Williams & Esteves (2017) do not explicitly recommend this metric, it was included in this study along with the maximum and minimum error, as several reference studies on Delft3D models have utilized these metrics (Amadori et al., 2021; Chanudet et al., 2012; Cardoso-Mohedano et al., 2019; Soulignac et al., 2018).

In this study, the processed telemetry data was unevenly distributed both spatially, across three dimensions, and temporally, over the simulation period. This introduces potential scale-dependent bias in RMSE and MAE across depths and time. To ensure scale-independent accuracy validation, the difference between simulated and observed data can be normalized relative to their individual mean and then divided by the standard deviation of the observed temperatures (Equation 16). This approach accounts for differences in value magnitude across spatial and temporal points and instead highlights the discrepancy between simulated and observed data in relation to variance, which remains independent of value magnitude across datasets (Amadori et al., 2021). This normalization approach, known as Normalized Centered Root Mean Square Deviation (NCRMSD), produces a dimensionless error, enabling more effective comparisons. However, it does not indicate whether the model tends to overestimate or underestimate, which is crucial for understanding the impact of parameter variations on the simulation. To address this, Mean Error (ME) was also calculated, as this bias metric is based on variation rather than value magnitude and therefore remains unaffected by temporal and spatial distribution biases (Equation 15).

$$SD = \sqrt{\frac{1}{n}\sum_{i=1}^{n}(O_i - \bar{O})^2}$$

Equation 12

$$RMSE = \sqrt{\frac{1}{n}\sum_{i=1}^{n}(S_i - O_i)^2}$$

Equation 13

$$MAE = \sqrt{\frac{1}{n}\sum_{i=1}^{n}|S_i - O_i|}$$

Equation 14

$$ME = \frac{1}{n}\sum_{i=1}^{n}(S_i - O_i)$$

Equation 15

$$NCRMSD = \frac{\sqrt{\sum_{i=1}^{n}[(S_i - \bar{S}) - (O_i - \bar{O})]^2}}{\sqrt{\sum_{i=1}^{n}(O_i - \bar{O})^2}}$$

Equation 16

Where O is observed temperature values at time i, S is the simulated values at time i, $\bar{O}$ is the mean of the observed values and $\bar{S}$ is the mean of simulated values.

Validation metrics were calculated for the entire simulation period and monthly, incorporating depth ranges to examine temporal and three-dimensional variations in accuracy. Receiver depths ranged from 17 to 97 meters and were divided into eight 10-meter intervals to ensure detailed validation throughout the water column. While this approach was designed to provide sufficient data for metric calculations, data density varied across intervals. Some depth ranges contained thousands of observations, while others, such as the 17–27 m interval, had significantly fewer. This limitation should be considered when interpreting results, as lower data density may influence the reliability of certain metrics.

To provide a comprehensive assessment of model performance, visual representations of the validation metrics and simulation output were generated using R and QUICKPLOT. Temperature profile output was visualized with individual temperature scales for each month to distinguish the depth of the thermocline.

4. Results

The results section of this report is divided into two parts. The first part outlines the pre-processing and validation of the telemetry data, while the second part presents the results, calibration, and validation derived from the simulation in Delft3D.

4.1 Validation of telemetry temperature data

Using a one-hour residence threshold for depth data filtering, validation against 260 receiver temperatures aligned with join threshold timestamps and depths produced the following error statistics: RMSE was 0.498°C, MAE was 0.477°C, the residual mean measured -0.266°C, and the SD surrounding the residual mean was 0.421°C. The minimum residual value was recorded as -0.79°C, while the maximum residual value reached 0.94°C. These validation metrics should be interpreted with the calculated residual uncertainty of ±0.71°C in mind, as this represents the expected measurement variability due to combined instrument errors. Testing a 20-minute residence threshold revealed a minor increase in error values, especially in the extremes of residuals, with the minimum and maximum values shifting by -0.4°C and +0.5°C, respectively. A residence threshold of 1.5 hours demonstrated no variation in error metrics compared to one hour. Residuals for the same receiver and timestamp exhibited distinct clustering patterns, as illustrated in Figure 5, when applying the one-hour residence threshold. Notably, residual variance on the same date was observed, with 0.41°C on April 21 and 0.26°C on March 1 for Char_1395047. Similarly, a residual variance of 0.31°C was noted on September 4 for Char_1395040.

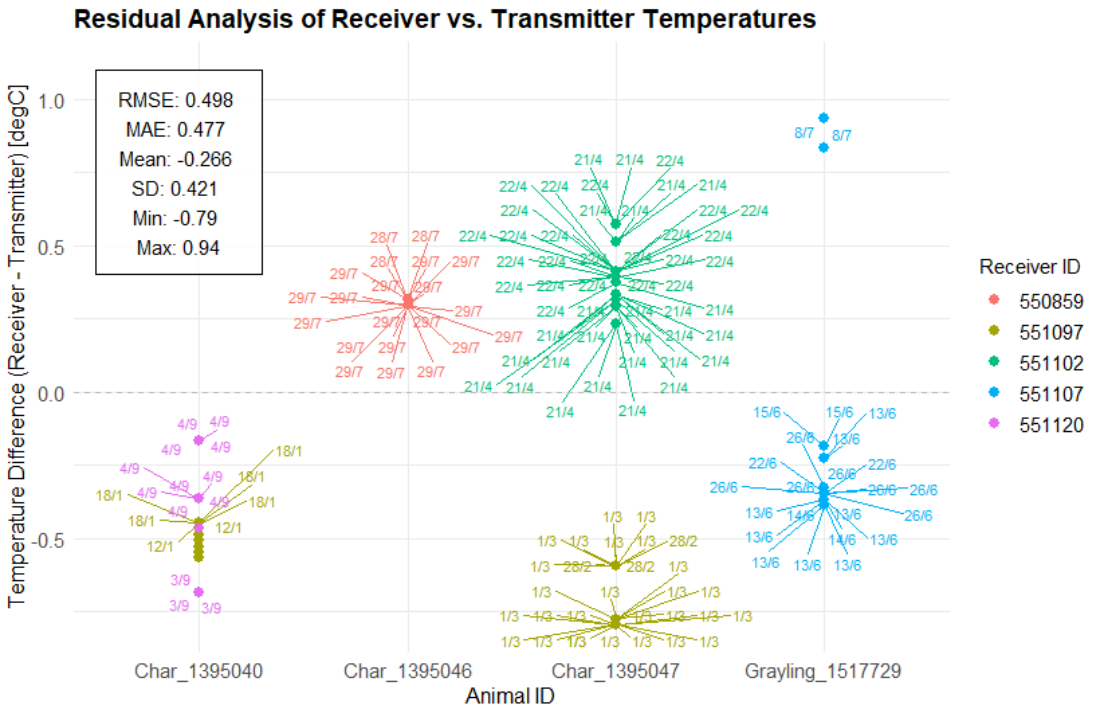

Figure 5: Telemetry transmitter temperatures were processed based on the fish residence time threshold for a fixed depth, where "fixed" refers to ±1m around the residence depth. The accuracy of the transmitter temperature measurements was validated by comparing receiver temperatures with transmitter temperatures recorded at the same receiver, depth, and timestamp (±5 minutes). The figure illustrates the residuals, i.e., the temperature difference between individual comparisons of receiver and transmitter temperatures, along with four statistical metrics and the residual range. These validation metrics should be interpreted with the calculated residual uncertainty of ±0.71°C in mind, as this represents the expected measurement variability due to combined instrument errors. A distinct clustering pattern is evident for the same receiver ID and date. Additionally, some variation in residual values is observed for Char_1395047 and Char_1395040.

4.2 Validation of simulated water temperatures

The maximum simulated flow velocity in the model output was 0.14 m/s. With the computational timestep of 60 seconds and the minimum grid cell size of 200 meters, the CFL number was calculated to be 0.042. This value is below the predefined stability limit of 0.6, which was set during model initialization. Therefore, the numerical stability criteria of the model was satisfied.

The validation metrics calculated for the annual values across all stations (see Table 5) showed an RMSE of 1.37°C, an NCRMSD of 2.04, an MAE of 1.05°C, and a ME of 0.19°C. The highest RMSE and MAE were observed in October, at 2.20°C and 1.72°C, respectively. ME indicated an overestimation of the simulated temperatures in all months except August, September, and October, where an underestimation was instead evident. In July and November, ME was close to zero. A sharp rise in ME occurred between November and December. The highest and lowest annual errors between simulated and observed temperatures were 9.29°C and -4.39°C, occurring at depth ranges of 77–87 m and 27–37 m, respectively, highlighting a considerable error range. Furthermore, the NCRMSD showed a very high error at depth range 17-25m. This coincided with a high overestimation according to ME.

Table 5: A Delft3D Flexible Mesh Suite model was developed for Lake Vättern, Sweden. The model was three-dimensional and simulated hourly lake water temperatures from January 1st, 2023, to December 31st, 2023. The model output was validated using spatially irregular telemetry receiver temperature measurements collected at varying temporal intervals. The table presents the validation results for four different metrics, both on a monthly basis, for the entire simulation period and for the receiver depths.

Month	**RMSE** [°C]	**NCRMSD** [-]	**MAE** [°C]	**Max Error** [°C]	**Min Error** [°C]	**ME** [°C]
Annual	1.37	2.04	1.05	9.29	-4.39	0.19
January	0.54	0.22	0.47	0.31	-1.15	0.46
February	0.73	0.26	0.65	0.27	-1.31	0.65
Mars	1.00	0.15	0.91	0.77	-1.60	0.90
April	0.66	0.50	0.64	-0.32	-1.58	0.64
May	0.68	0.44	0.56	0.51	-1.76	0.55
June	0.80	0.56	0.66	9.29	-2.16	0.64
July	1.19	0.76	0.96	4.77	-2.82	0.13
August	1.39	1.45	1.12	5.81	-3.31	-0.26
September	1.57	1.45	1.07	7.65	-2.48	-0.67
October	2.20	1.44	1.73	7.39	-4.39	-1.35
November	1.30	1.75	1.08	2.68	-2.59	0.02
December	1.75	1.05	1.58	0.53	-4.04	1.58
Depth						
17-27m	1.74	8.49	-0.20	-0.20	-2.53	1.51
27-37m	1.62	1.33	1.23	7.64	-4.39	-0.16
37-47m	1.02	1.23	0.91	0.51	-2.00	0.91
47-57m	1.01	0.51	0.92	-0.51	-1.33	0.92
57-67m	1.13	1.44	1.09	0.77	-1.40	0.32
67-77m	0.54	0.14	0.54	0.53	-0.55	0.01
77-87m	1.13	0.88	0.89	9.29	-2.83	0.38
87-97m	2.56	-	2.56	2.56	2.56	-2.56

When analysing the validation metrics per month and station in conjunction with depth, as shown in Figure 6 and 7, no discernible patterns emerged in the vertical dimension. Similarly, no clear spatial trends in the horizontal could be identified. However, a distinct temporal pattern was evident, where RMSE and MAE increased for certain stations from July until the end of the simulation period. The error pattern was also confirmed by the NCRMSD which showed increasing error for the same months (see Figure 7). ME followed a similar trend (see Figure 7), starting with low values at the beginning of the simulation period and continuing through July. Between July and October, some stations exhibited rising values, followed by a sharp decline toward the end of the simulation period. This suggested that the model tended to underestimate temperatures during the summer months, and overestimate temperatures otherwise.

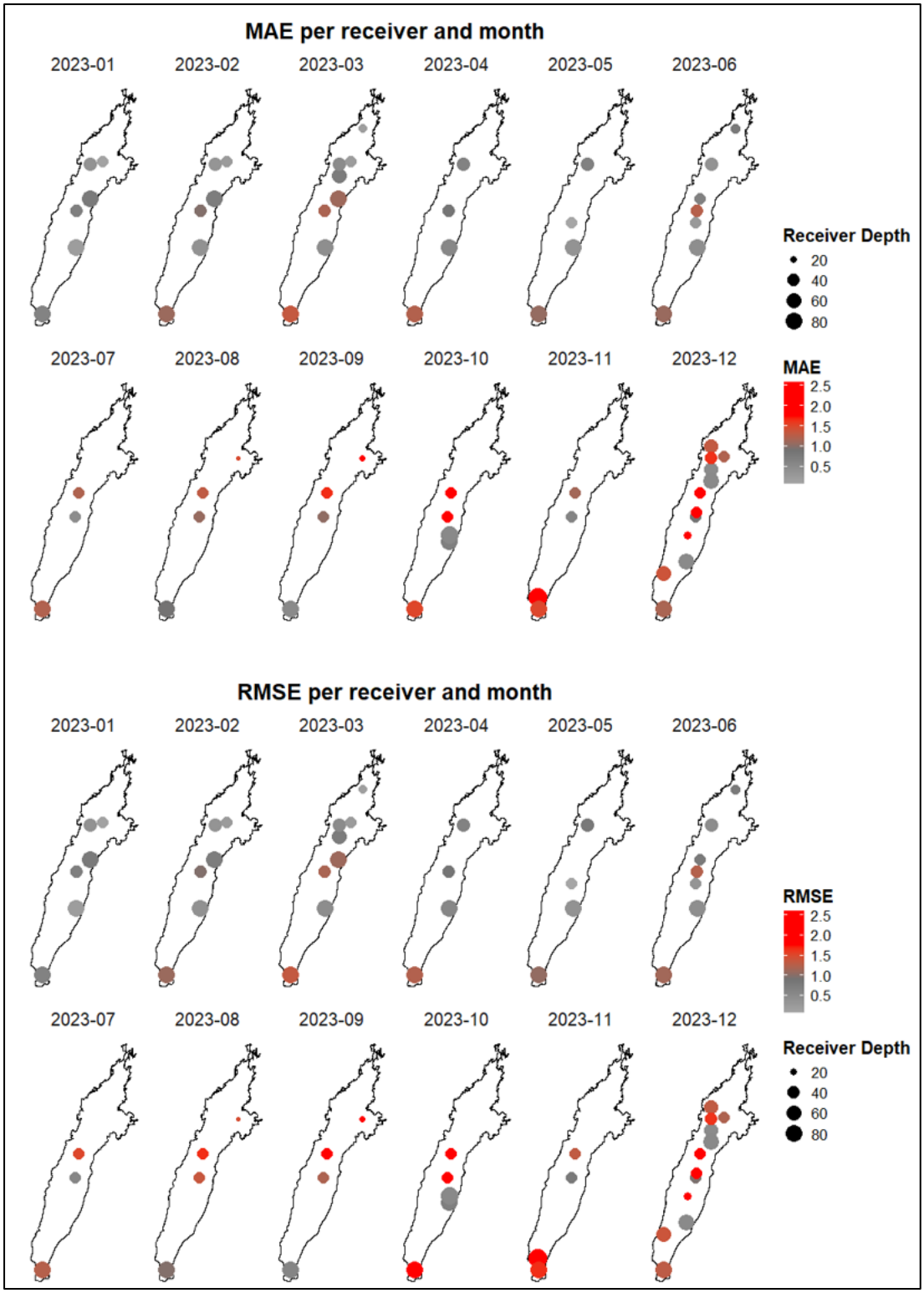

Figure 6: A Delft3D Flexible Mesh Suite model was developed for Lake Vättern, Sweden. The model was three-dimensional and simulated hourly lake water temperatures from January 1st, 2023, to December 31st, 2023. The model output was validated using spatially irregular telemetry receiver temperature measurements collected at varying temporal intervals. The figure visualizes the Residual Mean Squared Error (RMSE) and Mean Absolute Error (MAE) for each month. Receivers are represented as points, with a colour gradient indicating the error metric value. The depth of each receiver is illustrated by the size of the point. The purpose of the figure is to analyse spatial and temporal patterns in the errors.

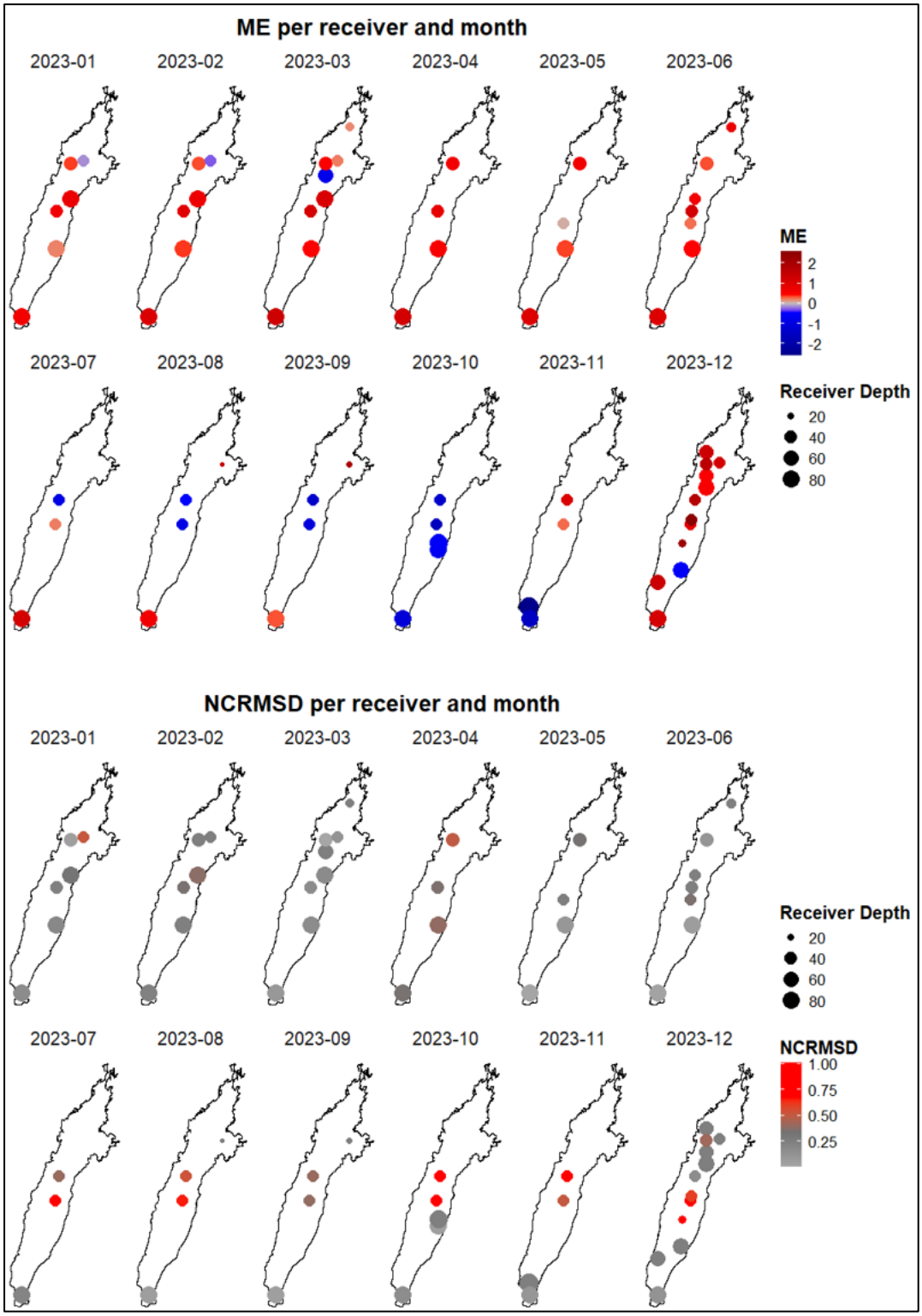

Figure 7: A Delft3D Flexible Mesh Suite model was developed for Lake Vättern, Sweden. The model was three-dimensional and simulated hourly lake water temperatures from January 1st, 2023, to December 31st, 2023. The model output was validated using spatially irregular telemetry receiver temperature measurements collected at varying temporal intervals. The figure visualizes the Normalized Centered Root Mean Squared Deviation (NCRMSD) and Mean Error (ME) for each month. Receivers are represented as points, with a colour gradient indicating the error metric value. The depth of each receiver is illustrated by the size of the point. The purpose of the figure is to analyse spatial and temporal patterns in the errors.

4.3 Vertical profiles of simulated water temperature

Figures 8 and 9 present vertical temperature profiles along a transect from the southern to the northern part of the lake. Note: The lake illustration has been rotated to enhance readability by using a larger figure! For an accurate geographical representation of the lake, see Figure 2. Data is shown for the 30th day at 12:00 in May, June, October, and November to capture the formation and dissolution of temperature stratification. By late May, density differences in the water column began to generate a notable temperature gradient between the bottom and the surface. This gradient did intensify by the end of June, forming a distinct transition between warmer surface water and colder deep water. The sharp thermal stratification remained until November, gradually dissipating by the end of the month, at which temperature differences where low across short vertical distances. In the shallower northern parts of the lake, water warms and cools more rapidly, preventing the development of stable stratification. Throughout the simulation period, the model output did not display structural anomalies, further confirming numerical stability.

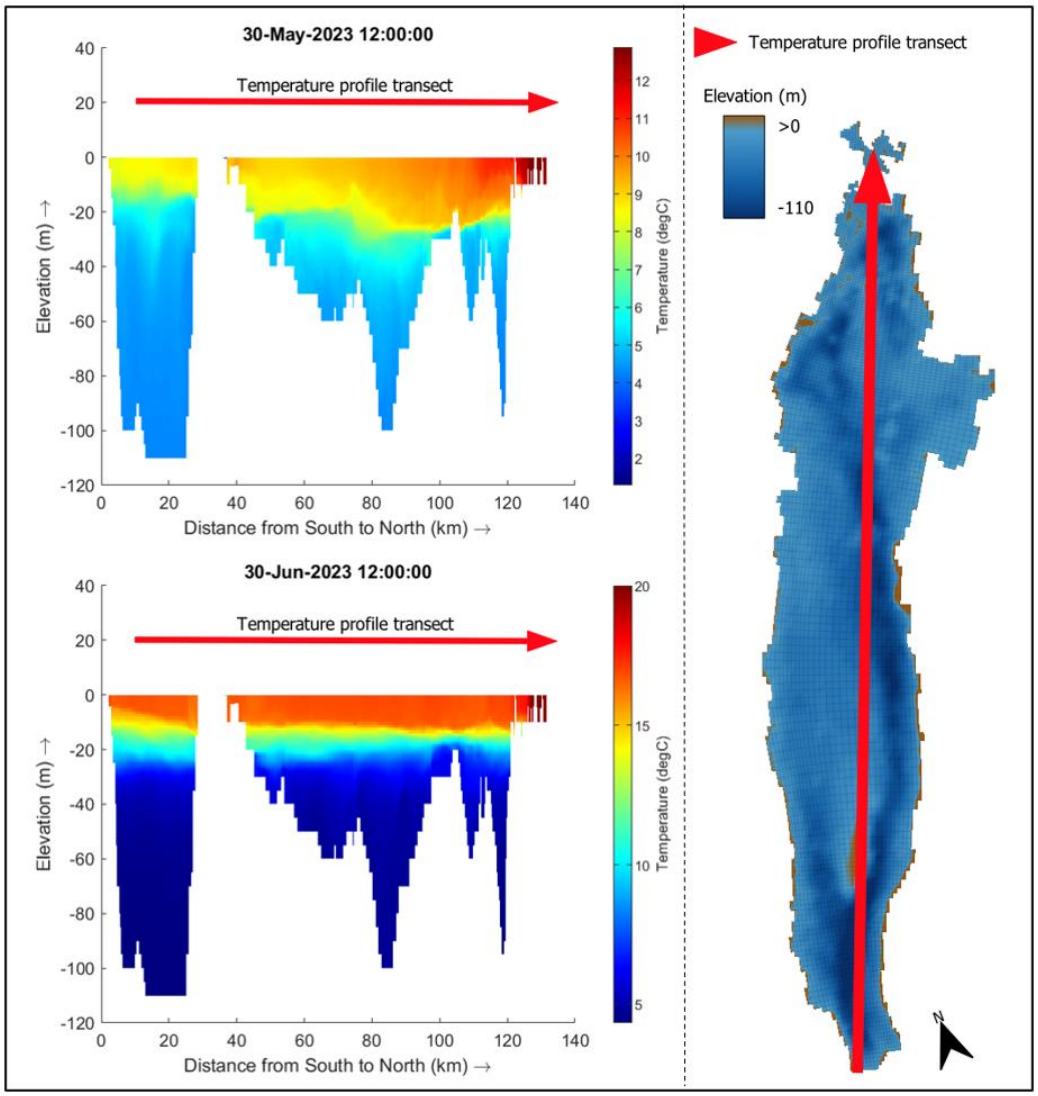

Figure 8: A Delft3D Flexible Mesh Suite model was developed for Lake Vättern, Sweden. The model was three-dimensional and simulated hourly lake water temperatures from January 1st, 2023, to December 31st, 2023. The figure illustrates vertical temperature profiles from the southern to the northern part of the lake (following the direction of the red arrow) at two time points, one month apart, highlighting the development of thermal stratification.

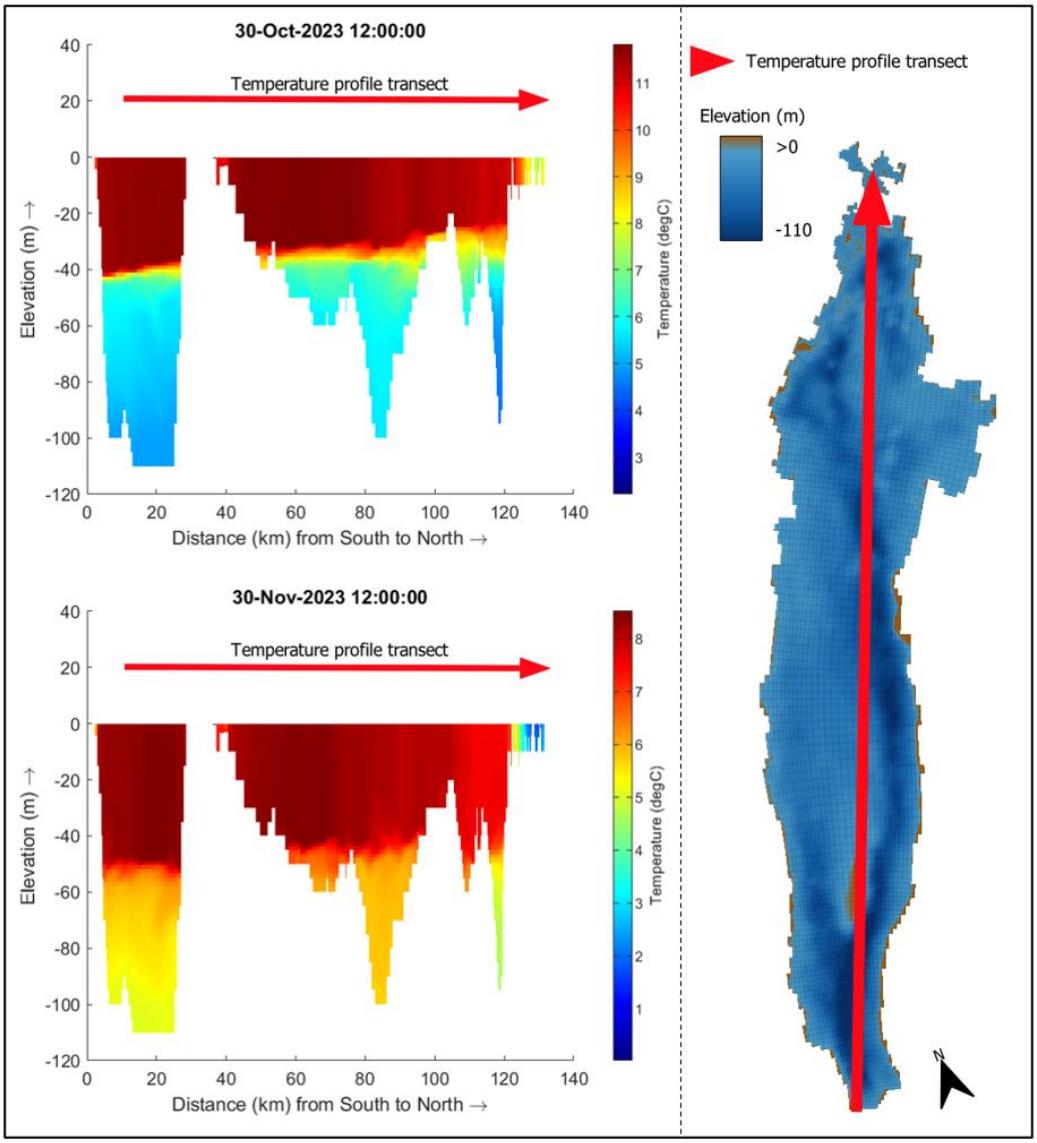

Figure 9: A Delft3D Flexible Mesh Suite model was developed for Lake Vättern, Sweden. The model was three-dimensional and simulated hourly lake water temperatures from January 1st, 2023, to December 31st, 2023. The figure illustrates vertical temperature profiles from the southern to the northern part of the lake (following the direction of the red arrow) at two time points, one month apart, highlighting the gradual mixing of water layers and dissolution of thermal stratification.

5. Discussion

5.1 Temperature measurements from telemetry data

The vertical migration errors in telemetry data, as described by Brownscombe et al. (2019), were mitigated by applying a threshold of one hour for residence time at a fixed depth. This approach was validated using data from an individual Arctic char (see Figure 4), which demonstrated that the one-hour depth residence threshold was sufficient to observe a stagnation in the temperature drop. This suggests that changes in residence depth do not significantly contribute to temperature measurement errors when this threshold is applied. Furthermore, validation against receiver temperatures indicated a slight deterioration in accuracy when a shorter residence time of 20-minutes were used, although the deterioration was mainly seen as higher residual variance. However, when residence time increased beyond one hour, validation metrics remained stable, reinforcing the effectiveness of the one-hour threshold in minimizing vertical migration-induced errors.

The residual error illustrated in Figure 5 exhibits a systematic pattern, characterized by distinct clustering at an error magnitude, associated with each transmitter in relation to both time and receiver position. The underlying causes of this systematic error likely stem from two primary factors. (1) Measurement uncertainty, where the total temperature residual uncertainty, calculated through error propagation, was determined to be ±0.71°C, and the depth uncertainty was ±0.5m to ±6.8m (see Table 2). (2) Spatial discrepancies occurring when a fish is positioned at a considerable distance from the receiver, potentially leading to temperature inconsistencies due to environmental variability within the detection zone. Although this study operates under the assumption of thermal homogeneity within each receiver's detection zone, reality is likely more complex. The large detection zone, spanning approximately 2 km, introduces possible variability in water currents, which in turn affects localized temperature conditions. Consequently, temperature readings at the receiver might not always reflect the actual environmental conditions experienced by the fish transmitter located at the receiver depth level.

One key conclusion derived from the clustering pattern in Figure 5 is that errors associated with vertical fish movements appear to be negligible after processing of the transmitter data. If vertical displacement was a significant source of error after applying the one-hour residence threshold, residuals for individual fish would exhibit substantial dispersion along the y-axis. This would be expected given the rapid vertical temperature gradients observed throughout much of the year (see Figures 8 and 9) and the vertical movement behaviour observed in Figure 4. However, variation in residual values was only observed in two fish, and this variance remained minor, within the sub-accuracy range of the telemetry instruments. Additionally, longer residence times would theoretically reduce residual dispersion if vertical movement were a dominant error source since it would give more time for the temperature lag to stagnate at a new depth. However, no such reduction was observed, suggesting that vertical movement is unlikely to have a significant impact beyond the one-hour threshold for the data used in this study.

The inability to filter horizontal movement may contribute to the observed minor residual variance, as depth-based thresholds effectively limit vertical displacement but cannot account for lateral migration across the receiver's detection zone. Nevertheless,

a shorter residence time at a fixed depth did result in increased residual variance, implying that vertical fish movement may influence error magnitude when residence time is insufficient. This highlights the importance of selecting an appropriate residence threshold to ensure reliable temperature measurements while accounting for fish behaviour.

5.1.1 Depth residence threshold compared with earlier studies

When reviewing previous research that used telemetry data for temperature measurements, no studies were found that explicitly integrated telemetry data with a threshold based on depth for transmitter temperature measurements. The only exception was the study by Bronscombe et al (2019) which only outlined the challenges that must be addressed before telemetry temperature data can be practically applied, with depth residence time being the most dominant concern. As a result, comparison with earlier studies was carried out exclusively with the study by Kristensen et al (2018). Their study used a very similar instrument to the telemetry transmitter with a temperature sensor surgically implanted in the fish abdominal cavity. That instrument was a G5 long-life archival DTS tag which stores the temperature and depth data in its internal memory rather than sending it to a receiver (CEFAS Technology, n.d.). The comparison with Kristensen et al (2018) is justified because their study utilized a temperature sensor that exhibits similar temperature lag effects due to depth changes, providing a comparable basis for evaluating the transmitter data used in this study.

The results in this study indicate that the 20-minute residence threshold applied by Kristensen et al. (2018) may have been too short to ensure stable temperature measurements. However, given that fish vary in size and that vertical temperature gradients fluctuate throughout the year, a one-hour threshold is unlikely to be universally optimal. Smaller fish with thinner abdominal walls likely experience shorter temperature update times compared to larger individuals. The fish studied here was a 75 cm Arctic char at the time of transmitter implantation, representing the largest specimen in the dataset. This suggests that the one-hour threshold approximates the maximum residence time requirement for this dataset, a conclusion further supported by the lack of accuracy improvement when a longer threshold was applied. This also suggests that the depth residence threshold is, in fact, influenced by the size of the fish. Furthermore, larger vertical temperature differences may necessitate longer thermal adjustment periods. For instance, cold-water fish migrating vertically for nighttime foraging, transitioning from deep cold waters to warmer surface layers above the thermocline (Flood et al., 2021), may require residence times exceeding one hour due to the substantial thermal disparity across depths.

While Kristensen et al. (2018) applied a 20-minute residence threshold in their study, there is no indication that they systematically evaluated its effectiveness as a general threshold. However, increasing the threshold reduces the available dataset, as fewer continuous depth chains meet the inclusion criteria before the fish moves again. Therefore, the residence threshold could beneficially be validated for each dataset to ensure data retention and methodological reliability. This study suggests that the same principle applies for when implementing the timestamp join interval between temperature and depth readings in telemetry data, addressing the issue of asynchronous recordings described by Brownscombe et al. (2019). When applying a ±5-minute timestamp join interval, as used in this study, temperature readings remained stable without exhibiting drastic changes (see Figure 3). Similarly, the 10-minute threshold

used for continuous depth residence time chains, together with the investigation of residence thresholds (see Figure 4), help assess depth-related movement patterns. If a fish moves between depths and returns to its original depth within the windows in the 10-minute depth residence time chain, the recorded temperature does not have time to change significantly. This potential source of error is not described by Kristensen et al. (2018). Likely due to a configuration alternative in the G5 long-life archival DTS tag where depth and temperature can be measured at the exact same timestamp with very short time intervals (CEFAS Technology, n.d.), eliminating the uncertainty of asynchronous recordings of depths and temperatures as well as the windows of data absence between depth records.

Each of the three thresholds applied in this study plays a crucial role in ensuring telemetry temperature accuracy. The ±5-minute timestamp join interval between depth and temperature readings ensures that naturally occurring temperature fluctuations do not cause mismatches in temperature recordings relative to depth timestamps. The 10-minute threshold for continuous depth residence time chains prevents short-duration vertical movements from influencing transmitter temperature recordings. Finally, the one-hour residence time threshold at a new depth ensures that the delay in transmitter temperature adjustment stabilizes once the fish remains static at a new depth, making the recorded temperature representative of that depth. Together, these thresholds enhance the reliability of temperature-depth associations and improve the precision of telemetry-based temperature measurements.

5.1.2 Telemetry transmitter temperatures and Delft3D model validation

A solution to the issue of horizontal temperature variations within detection zones, as described by Brownscombe et al. (2019), was not explored in this study. However, a fourth issue was identified during this study regarding compatibility with depth data, which is unique to this type of application and not previously addressed by Brownscombe et al. (2019). Instances where temperature measurements occasionally fall outside the three-dimensional range of depth data require special attention, as such measurements can result in erroneous simulation outcomes and errors. In this study, the exclusion of these observations was chosen as the most straightforward approach to minimizing errors in subsequent use of the dataset. Nevertheless, an alternative methodology exists that would preserve all observations within the dataset. Given that the detection zone spans 2 km and thermal homogeneity is assumed across this area, transmitter temperature readings recorded at depths exceeding those of the receiver could theoretically be reassigned to alternative locations within the detection zone, provided the depth does not exceed that of the transmitter. However, implementing this approach is inherently complex and would require a tailored programming solution, particularly when handling the extensive datasets typically associated with telemetry studies (Brownscombe et al., 2019).

After filtering the data, approximately 150,000 transmitter temperature readings remained, representing about one-third of the original dataset. Including receiver temperature measurements, a total of approximately 300,000 temperature observations remained after processing. Despite the filtering, a substantial portion of the 506,507 observations was thus retained due to the high detection frequency as also described by Brownscombe et al. (2019). The statistical validation of transmitter temperatures demonstrates robust overall accuracy, considering the residual uncertainty of ±0.71°C (see Figure 5). However, the significant variation observed in extreme residuals

warrants careful consideration. Since the validation of transmitter temperatures was based on only 260 measurements pairs out of 150,000 possible measurement pairs (≈ 0.17%), the extent of variation in extreme residuals may be greater for untested recordings. These discrepancies must be accounted for, particularly in studies that rely on transmitter temperature readings as benchmarks for validating other temperature measurements, as is the case in this study.

Due to this uncertainty, transmitter temperatures were excluded from the validation of the Delft3D model, relying solely on receiver temperature readings instead. This decision was made to ensure a fair evaluation of the beta version of the software and its output. If transmitter temperatures had been included, unknown discrepancies in their readings could have led to a misleading conclusion that the model performed poorly and false patterns in the validation could have been seen due to the spatial irregularity of the transmitter temperatures in combination with the unknown residual variance. Any perceived error in model validation may result from an unknown variance in transmitter temperature measurements rather than inaccuracies in the model itself. The validation of the model temperatures will still have to be seen in the light of the receiver temperature accuracy of ±0.5°C.

5.2 Delft3D Flexible Mesh Suite 2D3D model

5.2.1 Practical implementation

The creation of the irregular grid in the RGFGRID module proved to be a complex process due to the highly detailed land boundary of Lake Vättern. The high-resolution shoreline prevented automated grid generation from land boundary polylines, as intersecting grid lines formed across multiple cells, resulting in orthogonality values exceeding the threshold defined in the RGFGRID manual (Deltares, 2025c). Ensuring orthogonality in the grid is crucial for maintaining numerical stability and accuracy in the hydrodynamic simulations as a highly orthogonal grid minimizes computational errors and improves the reliability of flow and transport modelling (Deltares, 2025b). To resolve the issue and meet the orthogonality criteria, a semi-automated approach was used as described in section 3.4.1. At the time of this study, Deltares (n.d.) provides a standalone, Matlab-based graphical user interface known as DELFT DASHBOARD, which enables rapid automated irregular grid generation. However, an incompatibility between the required Matlab version for DELFT DASHBOARD and the Delft3D version used prevented its application in this project. Although this incompatibility limited the use of DELFT DASHBOARD in this study, Menten et al. (2023) successfully implemented the tool during their model setup. However, their study does not provide details on how they achieved this, suggesting that they either did not encounter the same compatibility issue, possibly due to differences in software versions, or managed to resolve it through an unspecified approach. Due to limited experience with alternative Matlab configurations, a manual approach was therefore chosen in this study to ensure grid stability. Furthermore, none of the referenced studies (Amadori et al., 2021; Bermúdez et al., 2018; Cardoso-Mohedano et al., 2019; Chanudet et al., 2012; Kranenburg et al., 2020; Schwindt et al., 2023; Sharaf et al., 2021; Soulignac et al., 2018) mention the use of DELFT DASHBOARD during grid generation. However, it remains unclear whether this absence is due to compatibility issues or other methodological choices. While grid stability may vary between studies due to differences in grid generation approaches, the strict orthogonality requirement imposed by Delft3D minimizes potential discrepancies in numerical output.

The model setup was straightforward in the GUI, where assigning parameters and adding time series data for meteorological inputs could be done easily. However, the wind data could not be used as grid data in the model. ERA5-Land hourly data of the x- and y-components of wind, and air pressure was downloaded at a 0.1° (°lat/°long) resolution and converted into grid time series files following the example files provided in the Delft3D manual (Deltares, 2025a), including the specified file format and extensions. Although the Delft3D GUI wizard successfully received the files and they appeared normal in the master definition file, the grid files caused simulation errors due to incorrectly structured file formats. To troubleshoot, grid files confirmed to be functional were downloaded from the Delft3D forum, where similar issues had been discussed (Deltares Forum, 2021). However, when these files were used in the model setup for this study, the same error occurred. Based on this, it was concluded that the issue with the wind and air pressure grid files was likely due to a bug in the beta version. As a workaround, all meteorological data, including wind and air pressure, were used as time series files with uniform values across the lake's extent. This approach was not optimal, as temperature dynamics is largely influenced by meteorological parameters, which naturally varies across the 130 km long surface of Lake Vättern.

The assumption that the wind grid error stemmed from a beta version bug was further supported by the simulation results. When the model was run in the GUI, the simulation appeared to proceed normally for 12 hours, and according to the diagnostics file, it reached a normal end. However, upon examining the output in Delft3D QUICKPLOT, the three-dimensional grid was fragmented, with large subsurface areas missing output values. Further troubleshooting led to the discovery of a short note in the Delft3D manual stating that the beta version GUI used in this study had limited functionality for three-dimensional simulations (Deltares, 2025a). To address this, the model was exported to a DIMR configuration file and run via a batch script within the installation directory. This approach successfully produced an output file after a similar runtime of 12 hours and without fragmentation, confirming that three-dimensional simulations inside the Delft3D GUI was not fully functional at the time of this study. Due to a misconfiguration in OpenMP, only 23 threads were utilized when the simulation was runed outside the GUI, whereas 32 threads were used within it. Given that the computer had 48 available threads (two per core), a correctly configured setup might have reduced the simulation runtime to under 12 hours.

Deltares (2025a) suggests using OpenDA to calibrate the model by systematically testing all adjustable parameters to identify those that yield optimal performance. OpenDA is an open-source platform for data assimilation and calibration that is compatible with Delft3D. It manages model input, retrieves simulation output, and compares it against observed temperature data to determine the most suitable parameter settings for the lake model. However, due to the narrow timeframe of this project and limited experience with this configuration, implementing OpenDA was considered too complex. Instead, reference was made to Amadori et al. (2021) and their model setup, as well as the sensitivity analysis conducted by Chanudet et al. (2012). Amadori et al. (2021) utilized OpenDA for their calibration, which further supports the use of their parameters in this study, given the physical similarities between the lakes. While OpenDA was also employed by Menten et al. (2023), no other reference studies besides Amadori et al. (2021) used OpenDA for parameter calibration (Bermúdez et al., 2018; Cardoso-Mohedano et al., 2019; Chanudet et al., 2012; Kranenburg et al., 2020;

Schwindt et al., 2023; Sharaf et al., 2021; Soulignac et al., 2018). This suggests that, despite being the recommended approach by the Delft3D software developer, OpenDA presents practical challenges that limit its widespread adoption.

Consequently, alternative calibration methods have been explored in the reference studies to achieve reliable parameters. Chanudet et al. (2012) conducted a sensitivity analysis using an iterative manual approach to assess the influence of parameters on water temperature. While this method likely required substantial time and effort, it provided a more controlled and transparent evaluation of parameter sensitivity and allowed for a more tailored parameter selection compared to relying on values from previous studies, as done in this study. However, errors in the simulation output when run within the GUI prevented manual calibration due to the narrow timeframe and the long simulation runtime.

5.2.2 General Performance of the Delft3D model

The MAE for the entire simulation period across all depths was 1.05°C, exceeding the upper range of values reported in previous studies, which found MAE between 0.1°C and 1.02°C (Amadori et al., 2021; Cardoso-Mohedano et al., 2019; Chanudet et al., 2012; Sharaf et al., 2021; Soulignac et al., 2018). The error range in this study was extensive, spanning from -4.39°C to 9.29°C, reflecting substantial variability in model deviations (see Table 5). RMSE for the entire simulation period was 1.37°C, with monthly values ranging from 0.54°C to 2.20°C. While Dissanayake et al. (2019) reported an RMSE of 4°C and Schwindt et al. (2023) reported an RMSE of 5.24°C, this metric represents the average squared error, meaning larger individual errors disproportionately influence its magnitude (see Equation 13). However, RMSE alone does not necessarily confirm the presence of extreme individual errors higher than RMSE, as the distribution of errors also plays a crucial role in this metric. Schwindt et al. (2023) validated their model using a vertical temperature profile at a single timestamp, with a significantly shorter simulation period of only seven days in August. Given that thermal stratification during this period leads to high variability in temperature profiles, the validation may not have adequately captured the model's ability to simulate turbulence. This could have led to a misinterpretation of the model's performance, wrongly suggesting poor accuracy. Consequently, the high RMSE in their study likely stems from the limited number of validation points both spatially and temporally, rather than reflecting actual deficiencies in model performance, an issue acknowledged in the study (Schwindt et al., 2023).

As the validation data originates from varying numbers of observation points, sampling depths, and temporal intervals across different lake sizes in the reference studies (see Table 6), direct comparisons may be misleading. Differences in spatial and temporal resolution, as well as the variability in measurement approaches, could influence error metrics and model assessments, making it essential to contextualize findings rather than relying on a one-to-one comparison.

Since all reference studies in Table 6 assess model accuracy in the vertical dimension and all lakes exhibit seasonal stratification, lake depth may be less critical for comparing validation methods. However, the sampling depth interval within the water column is highly relevant, as it affects the accuracy of capturing vertical turbulence effects. Lake size is another key factor, as it influences the density of observation points (point with a known ground truth temperature), which determine the extent to which

depth-dependent temperature variations are captured. The number of observation points varies across studies without a systematic increase with lake size. For instance, the largest lake studied (2,700 km²) was validated with three observation points (Kranenburg et al., 2020), the same number used by Sharaf et al. (2021) for a much smaller lake (12 km²). Additionally, Sharaf et al. (2021) incorporated satellite data, increasing the horizontal sample density compared to Kranenburg et al. (2020).

Table 6: A Delft3D Flexible Mesh Suite 2D3D model was set up and executed. The output was then compared to previous studies that used Delft3D for water temperature simulation. The table provides a nuanced comparison of the validation data from these reference studies, emphasizing the number of observation points, depth ranges, and temporal intervals.

Study	Lake surface area	Observation points	Depth interval	Temporal interval
Soulignac et al., (2018)	580km^2	2	Interpolated from two depths (0m and 30m)	Monthly
Amadori et al., (2021)	368km^2	19 - merged by stations and satellite data	Varying between 0-330m across observation points	Varying between hourly-monthly between observation points
Cardoso-Mohedano et al., (2019)	3.15km^2	1	4m, 10m, 25m, 32m and 56m	30-minutes
Dissanayake et al., (2019)	470km^2	1	28 depths between 0.8m and 125m	60 seconds
Schwindt et al., (2023)	0.88km^2	1	Continuous vertical profile	One time during simulation period
Sharaf et al., (2021)	12km^2	3 and satellite surface temperatures	1m, 4m, 7m, 10m, 13m and 16m	Not stated
Chanudet et al., (2012)	450km^2	9	0.5m – 1m	Weekly
Kranenburg et al., (2020)	2700km^2	3	Interpolated from 0m-70m with 10m intervals	5min

The differences outlined in Table 6 underscore the importance of comparing scale-independent validation metrics that account for variations in the number, spatial distribution, and temporal spread of observation points.

5.2.3 Scale-independent evaluation of the Delft3D model

Among the reviewed studies, only Amadori et al. (2021) normalized their validation metrics to address scale differences in their approach. This is unsurprising, as Amadori et al. (2021) had the highest number of observation points and data sources of all reference studies (see Table 6), necessitating a normalized validation method. They employed NCRMSD to assess the magnitude of error and ME to determine whether the model tended to over- or underestimate temperatures compared to ground truth. The

study utilized a wide range of in situ and remotely sensed temperature data to compile an extensive set of ground truths. Given the large number of sources, 12 in total, including historical project measurements, station-based time series, and thermal satellite data, the validation dataset was fragmented. It varied in both three-dimensional and temporal resolution throughout the simulation period. This fragmentation is also present in this study, where the receiver data, after filtering, remains temporally and spatially discontinuous. Given the high similarity in validation data and the physical similarities between their studied lake and Lake Vättern, particularly in terms of shape, orientation and depth, the results from Amadori et al. (2021) provide an especially relevant basis for direct comparison.

However, there are key differences that need to be outlined. Firstly, the surface area of Lake Vättern is 6376 km² compared to 368 km² of the lake studied by Amadori et al. (2021). Despite Lake Vättern having 57 receivers, this discrepancy in size results in a significant difference in observation point density with about five times more observation points in relation to surface area for Amadori et al. (2021) during the entire simulation periods. Additionally, this study lacks vertical insight at any of the observation points, relying solely on static depth observations for validation at every observation point. In contrast, Amadori et al. (2021) incorporated vertical profiling in 8 out of 12 observation points, enabling a more refined assessment of the model's ability to capture turbulence. Lastly, Amadori et al. (2021) does not calculate error propagation when using all the validation datasets but rather evaluates the model result with each dataset, thus avoid mixing different instrument accuracies. That is not a difference to the receiver data used in this study but an important part to clarify when comparing the results between studies as there will be an accuracy difference among the validation data used by Amadori et al. (2021). The differences and key knowledge in validation encompass several aspects, but the three mentioned are the most pronounced in a direct comparison.

NCRMSD and ME ranged from 0.25 to 1.37 and -0.57°C to 1.47°C, respectively, across all datasets and depths in the validation by Amadori et al. (2021). Since the datasets in Amadori et al. (2021) cover different time periods, a scale-independent comparison can be made with the monthly NCRMSD and ME in this study, which range from 0.22 to 1.75 and -1.35°C to 1.58°C, respectively (see Table 5). This direct comparison indicates that the Delft3D model setup in this study performs poorer than the reference study and tends to both overestimate and underestimate temperatures at a higher magnitude.

The largest NCRMSD observed by Amadori et al. (2021) is in simulated water between the epilimnion and hypolimnion where the temperature exhibits the highest variation. Since the lake in that study is a lake exhibiting summer stagnation, the highest NCRMSD also have a temporal pattern in the error directly connected to the stratification period. These patterns are seen also in this study where NCRMSD increases in July and remains high throughout the simulation period (see Table 5), although the error magnitude is significantly smaller for Amadori et al. (2021). The two stations exhibiting the highest NCRMSD in Figure 7 during the summer months is located at a depth of 37m. When examining the thermocline in Figure 8 in the end of June, the thermocline is located higher in the water column than 37m. What this temporal snapshot does not show is the fluctuations in thermocline depth across timestamps where wind occasionally pushes down the thermocline deeper in the water column, also explained by Flood et al. (2021). This is important to consider when

comparing the error metrics at a depth for an entire month (see Figure 7) with the figures of the temperature profile (see Figure 8), as these wrongly could suggest that a receiver does not exhibit the rapid temperature gradient in the thermocline. Thus, during the summer months, the receiver located at 37m will exhibit higher variation in temperatures than receiver located much deeper, or much shallower than the thermocline. A higher NCRMSD at this depth implies that the model fails to capture this variability and thus fails to simulate the turbulence effects.

5.2.4 Sources of errors and performance issues in the Delft3D model

The annual NCRMSD of 8.49 in the depth interval of 17–27 m, which corresponds to the thermocline depth at the end of June (see Figure 8), stems from an insufficient number of observations at those receivers for a valid NCRMSD calculation. With only six measurements spread across five months, including two in December, the high variability results in a mean that does not accurately represent the observed fluctuations, leading to an exceptionally high NCRMSD at this depth interval. Despite the limited number of measurements, they still offer some insight into the model's ability to capture turbulence during summer, though not from a statistically robust perspective. By examining MAE and ME in Figure 7, two of these receivers appear as small data points in August and September, indicating an overestimation of simulated temperatures relative to ground truth by approximately 2°C. Since there is only one single observation available for comparison at each point, MAE simply reflects the absolute difference. Although it lacks statistical significance, this remains the only available insight into the model's performance at this depth interval. Despite the limited number of observations, they still provide indications of how turbulence is simulated. Without these data points, any assessment of the model's behavior in this specific layer would be entirely absent.

Amadori et al. (2021) observed an overestimation of bottom turbulence during winter months, a phenomenon also reported in other studies modeling three-dimensional lake temperatures in deep lakes (Råman Vinnå et al., 2017). This overestimation is attributed to prolonged and intense wind-driven mixing, combined with underestimated air temperatures, which leads to excessive bottom turbulence rather than the buoyancy-driven mixing that typically governs deep-water circulation in deep lakes. As a result, the model erroneously simulates complete vertical mixing during winter, a process that does not actually occur. The resulting temperature underestimation stems from cold surface water being mixed deeper into the lake during simulation, reducing temperatures and causing the model to predict values lower than those observed. In summer, an overestimated wind stress is expected to force the thermocline deeper into the water column during simulation, leading to an overestimation of temperatures at greater depths during model validation.

In the case of Lake Vättern, the use of spatially uniform hourly wind data could exacerbate inaccuracies if overestimated, potentially reducing the model's reliability in deeper waters during summer and failing to capture winter mixing dynamics, as observed by Amadori et al. (2021). However, an examination of Figure 7, Table 5, and the annual variation in ME reveals a clear overestimation of temperatures from January through July. At this point, the model transitions to underestimating temperatures, coinciding with the onset of the stratification period, during which a distinct density change occurs at the end of June (see Figure 8). This underestimation persists throughout the summer, peaking in October and November as stratification begins to

dissipate (see Figure 9). By December, when stratification no longer exists in the model, temperatures are once again overestimated, mirroring the pre-summer pattern. This trend contrasts with Amadori et al. (2021), and the excessive winter bottom turbulence observed for some years when their model performed poorly. Based on these observations, it appears that the wind data used in this study is not overestimated, and the air-temperature data is not underestimated, despite being spatially uniform across the lake. Consequently, the likelihood of significant errors originating from flaws in meteorological forcing is reduced, as the direction of error does not indicate unrealistically high mixing and aligns with patterns observed in other successful models of simulated annual temperatures (Amadori et al., 2021; Råman Vinnå et al., 2017). The direct comparison with the model results acquired by Amadori et al. (2021) instead suggest that the calibratable parameters used as template in this study was not optimal for Lake Vättern.

5.3 Limitations and recommendations for future studies

The temperature lag analysis was based on a single fish, using a one-hour threshold derived from the largest individual in the dataset. Consequently, only one magnitude of depth change was examined. Furthermore, the analysis relied on telemetry data from a single year, limiting the scope and potential robustness of the findings. Future research could employ a more tailored approach by analyzing telemetry data over multiple years and possibly identify cases of depth changes from fish of varying sizes. This would allow for a species-length-specific depth residence thresholds analysis, improving transmitter data retention. Additionally, investigating depth changes of varying magnitudes across seasons could also help develop a dynamic framework of thresholds rather than a generalized model. Another possible approach is to test the lag time of transmitters in a lab environment. Such an approach would have the potential to completely reduce the uncertainty around lag-time in telemetry temperature measurements. However, there are challenges to overcome in the lab environment. These include how to artificially mimic different thicknesses of abdominal walls which would represent different sizes of fish, but also to mimic the movement in the natural temperature gradient found in lakes due to thermal stratification. Nevertheless, a controlled lab test would have the potential to reduce lag-time errors with high statistical accuracy.

After utilizing receiver data to validate the Delft3D model, a more comprehensive understanding of its capabilities and limitations emerged. The primary challenge in validating the Delft3D model in this study, using receiver data from Lake Vättern, is the limited number of receivers active at the thermocline depth during summer stagnation compared to wintertime (see Figures 6, 7, 8, and 9). Since turbulence is the primary driver of temperature dynamics, assessing the model's ability to simulate the thermocline provides the most insightful evaluation of its performance. Consequently, validation in this study primarily focuses on water column segments expected to yield the highest accuracy, as temperature variability is minimal below the thermocline. Given this, a higher error than observed could be assumed, and a possible calibration process lacking insight into model behaviour at thermocline depth would be challenging.

If transmitter temperature data could be further validated by incorporating a larger proportion of observations, it could serve as a valuable complement to receiver data. Since fish transmitters operate at varying depths, they could broaden vertical insight at

each observation point, potentially generating ground truth data at thermocline depth. The validation of transmitter temperatures in this study was determined to be statistically insignificant for the dataset, and thermal uncertainty within the 2 km buffer zone was deemed too high. It is important to acknowledge that telemetry data characteristics vary across lakes depending on depth and the number of receivers and transmitters, meaning the shortcomings observed in this study may not necessarily apply elsewhere.

To improve the statistical robustness of transmitter validation, it is necessary to assess horizontal temperature fluctuations in the receiver detection zone. Such analysis could confirm or contradict the possibility that extreme residuals in the validation process are caused by temperature variations inside the detection zone. However, validating transmitter data likely requires additional in-situ data than only the receiver data used in this study, which is historically absent for Lake Vättern. A combined approach integrating telemetry with other data collection methods in the future would enhance spatial and temporal resolution and improve calibration and validation of three-dimensional hydro-thermodynamic models. Alternatively, a higher measuring frequency than hourly in the receivers would enable higher possibilities of pairing receiver and transmitter timestamps, thus increasing the transmitter validation data when receiver temperatures serve as ground truth. A higher spatial density of receivers would also require a smaller detection zone, eliminating possible transmitter error sources with horizontal temperature heterogeneity. These suggestions would possibly broaden the usage of telemetry data, increasing its value in hydro-thermodynamic applications.

The author's limited calibration experience using OpenDA posed a challenge in achieving a high-performing Delft3D model in this study. Combined with time constraints, this necessitated using parameters from previous studies as templates, which the model’s accuracy and behavior indicate may be suboptimal. Parameter calibration tailored to this specific model could likely enhance performance. Although the validation data restricts a full assessment of the model’s ability to capture turbulence, it suggests insufficiencies. Therefore, calibration should prioritize turbulence-related parameters, guided by sensitivity analysis.

6. Conclusion

This study demonstrates that telemetry data, when present in a lake, have the potential to serve as ground truth for validating three-dimensional physical hydrodynamic models driven by meteorological data. However, the applicability of telemetry temperatures likely varies between lakes depending on the spatial distribution of receivers, particularly whether they are positioned at thermocline depth during summers. In this study, receiver density was highest in deeper waters beneath the thermocline, where physical models naturally exhibit lower error due to reduced temperature variance. Only two of 57 receivers were positioned at 17–27 meters, capturing the stratification process. The limited number of observations at these depths prevented statistically stable conclusions about the accuracy of the Delft3D model used in this study. Consequently, validation of the simulated temperatures and comparison to other studies relied on data that did not capture the most critical aspects of the simulation.

The transmitter temperatures showed promising potential as an additional validation tool in the telemetry dataset. However, an extensive pre-processing approach was required to filter out temperature measurements that did not accurately represent their registered depths. By accounting for lag-time effects shown by the longest fish individual in the dataset, where transmitter temperatures required approximately one hour to stabilize after depth changes by the fish, the accuracy demonstrated promising results. However, this lag-time is expected to vary between fish, depth change magnitude and temperature difference between the depths. Additionally, the validation was done with a very small fraction of the entire transmitter dataset (≈0.17%), adding uncertainty to the validation. Ultimately, transmitter temperature data were excluded from validating the Delft3D model due to insufficient statistically stable measurements and the presence of high residuals, which may have compromised the reliability of the model validation.

The comparison of the Delft3D model accuracy with other studies required a nuanced approach that balanced differences and similarities across research. Most notably, many studies lacked sufficient validation data sources, and the magnitude of validation data differed greatly between studies. This further confirms that in situ data remains a major limitation in model validation. The differences led to varying approaches in validation metrics, where some studies had to normalize data due to spatial and temporal spread, while others did not. A direct comparison was made with the results presented by Amadori et al. (2021) using scale-independent metrics. These metrics suggested that the model in this study performed poorer than the reference study. However, the largest deviations in error were attributed to shortcomings in the validation data rather than model performance. These include the limited number of measurements in the 17–27m interval and the use of static depth ground truth measurements at each observation point. Additionally, during model setup, a bug in the Delft3D version required uniform wind data across the lake extent. The comparison with observations from Amadori et al. (2021) suggests that this uniform wind input did not significantly impact model performance. Instead, the validation suggests that error could be reduced by calibrating model parameters to enhance turbulence representation, ideally using the OpenDA approach recommended by the software developer (Deltares, 2025a). However, this calibration would require more validation data at thermocline depths than was used in this study to achieve statistical stability. This challenge might be addressed through

further analysis of transmitter temperatures, which consist of a potentially large number of reliable measurements across the depth gradient.

References

Amadori, M., Giovannini, L., Toffolon, M., Piccolroaz, S., Zardi, D., Bresciani, M., Giardion, C., Luciani, G., Kliphuis, M., Haren, H. & Dijkstra, H. A. (2021). Multi-scale evaluation of a 3D lake model forced by an atmospheric model against standard monitoring data. *Environmental Modelling & Software*, *139*, 105017. https://doi.org/10.1016/j.envsoft.2021.105017

Angeler, D. G., Allen, C. R., Birgé, H. E., Drakare, S., McKie, B. G., & Johnson, R. K. (2014). Assessing and managing freshwater ecosystems vulnerable to environmental change. *Ambio*, *43*, 113-125. DOI: https://doi.org/10.1007/s13280-014-0566-z

Bek, M. A., Lowndes, I. S., Hargreaves, D. M., & Negm, A. M. (2019). Basics of lake modelling with applications. *Egyptian Coastal Lakes and Wetlands: Part I: Characteristics and Hydrodynamics*, 215-239. ISBN: 978-3-319-93589-8

Beletsky, D., Saylor, J. H., & Schwab, D. J. (1999). Mean circulation in the Great Lakes. *Journal of Great Lakes Research*, *25*(1), 78-93. DOI: https://doi.org/10.1016/S0380-1330(99)70718-5

Bermúdez, M., Cea, L., Puertas, J., Rodríguez, N., & Baztán, J. (2018). Numerical modeling of the impact of a pumped-storage hydroelectric power plant on the reservoirs' thermal stratification structure: a case study in NW Spain. *Environmental Modeling & Assessment*, *23*, 71-85. DOI: 10.1007/s10666-017-9557-3

Boehrer, B., & Schultze, M. (2008). Stratification of lakes. *Reviews of Geophysics, 46*(2). DOI: https://doi.org/10.1029/2006RG000210

Bouffard, D., & Wüest, A. (2019). Convection in lakes. *Annual Review of Fluid Mechanics*, *51*(1), 189-215. DOI: https://doi.org/10.1146/annurev-fluid-010518-040506

Brownscombe, J. W., Lédée, E. J., Raby, G. D., Struthers, D. P., Gutowsky, L. F., Nguyen, V. M., Young, N., Stokesbury, M. J. W., Holbrook, C.M., Brenden, T. O., Vandergoot, C. S., Murchie, K. J., Whoriskey, K., Flemming, J. M., Kessel, S. T., Krueger, C. C., & Cooke, S. J. (2019). Conducting and interpreting fish telemetry studies: considerations for researchers and resource managers. *Reviews in Fish Biology and Fisheries*, *29*, 369-400. DOI: https://doi.org/10.1007/s11160-019-09560-4

Cardoso-Mohedano, J. G., Sanchez-Cabeza, J. A., Ruiz-Fernández, A. C., Pérez-Bernal, L. H., Lima-Rego, J., & Giralt, S. (2019). Fast deep water warming of a subtropical crater lake. *Science of The Total Environment*, *691*, 1353-1361. DOI: 10.1016/j.scitotenv.2019.07.183

CEFAS Technology. (n.d.). *G5 long life archival DTS tag*. Retrieved 2025-05-27 from https://cefastechnology.co.uk/products/data-storage-tags/g5

Chanudet, V., Fabre, V., & van der Kaaij, T. (2012). Application of a three-dimensional hydrodynamic model to the Nam Theun 2 Reservoir (Lao PDR). *Journal of Great Lakes Research*, *38*(2), 260-269. DOI: 10.1016/j.jglr.2012.01.008

Chorin, A. J. (1967). The numerical solution of the Navier-Stokes equations for an incompressible fluid. *Bulletin of the American Mathematical Society*, *73*(6), 928-931. DOI: https://doi.org/10.1090/S0002-9904-1967-11853-6

Copernicus Climate Change Service, Climate Data Store, (2023): ERA5 hourly data on single levels from 1940 to present. Copernicus Climate Change Service (C3S) Climate Data Store (CDS), DOI: 10.24381/cds.adbb2d47

Deltares. (2024a). *D-Flow Flexible Mesh: Computational Cores and User Interface User Manual (*Version 2025*,* Revision 79761*).* Deltares systems.

Deltares. (2024b). *D-Flow Flexible Mesh: Technical Reference Manual* (Version 2025, Revision 79761). Deltares systems.

Deltares. (2024c). *RGFGRID: Generation and Manipulation of Structured and Unstructured Grids, Suitable for Delft3D-FLOW, Delft3D-WAVE, or D-Flow Flexible Mesh User Manual (*Revision 79761, Version 7.00*).* Deltares systems.

Deltares. *Processing tools*. Retreived 2025-05-21 from https://oss.deltares.nl/web/delft3d/pre-processing-tools

Deltares Forum (2021). *Adding wind vectors trough .wnd or .amv/.amu files.* [Forum thread]. Retreived 2025-04-19, from https://oss.deltares.nl/web/delft3dfm/forum/-/message_boards/message/4391639

European Centre for Medium-Range Weather Forecasts. (n.d.). *ERA5: Fifth generation of ECMWF atmospheric reanalyses of the global climate*. Copernicus Climate Data Store (CDS). Retrieved 2025-03-24, from https://cds.climate.copernicus.eu/datasets/reanalysis-era5-single-levels?tab=download

ESA Climate Change Initiative (CCI) Lakes: European Space Agency. (2024). *ESA Lakes Climate Change Initiative (Lakes_cci): Lake products, Version 2.1*. ESA Climate Office. Retrieved March 19, 2025, from Lakes

Fantner, G. (2013). *A brief introduction to error analysis and propagation*. École Polytechnique Fédérale de Lausanne (EPFL). Retreived 2025-05-18, from https://www.epfl.ch/labs/lben/wp-content/uploads/2018/07/Error-Propagation_2013.pdf

Flood, B., Wells, M., Dunlop, E. & Young, J. (2021). Vertical oscillations of the thermocline caused by internal waves modify coldwater pelagic fish distribution: results from a large stratified lake. *Journal of Great Lakes Research, 47*(5), 1386-1399. DOI: 10.1016/j.jglr.2021.06.010

Herb, W. R., & Stefan, H. G. (2005). Dynamics of vertical mixing in a shallow lake with submersed macrophytes. *Water Resources Research*, *41*(2). DOI: https://doi.org/10.1029/2003WR002613

Hersbach, H., Bell, B., Berrisford, P., Biavati, G., Horányi, A., Muñoz Sabater, J., Nicolas, J., Peubey, C., Radu, R., Rozum, I., Schepers, D., Simmons, A., Soci, C., Dee, D., Thépaut, J-N. (2023): ERA5 hourly data on single levels from 1940 to present. Copernicus Climate Change Service (C3S) Climate Data Store (CDS), DOI: 10.24381/cds.adbb2d47

Imboden, D. M., & Wüest, A. (1995). Mixing mechanisms in lakes. In *Physics and chemistry of lakes* (pp. 83-138). Berlin, Heidelberg: Springer Berlin Heidelberg. ISBN: 978-3-642-85134-6

Junzeng, X. U., Qi, W. E. I., Shizhang, P. E. N. G., & Yanmei, Y. U. (2012). Error of saturation vapor pressure calculated by different formulas and its effect on calculation of reference evapotranspiration in high latitude cold region. *Procedia Engineering*, *28*, 43-48. https://doi.org/10.1016/j.proeng.2012.01.680

Kangur, K., Ginter, K., Kangur, A., Kangur, P., & Möls, T. (2020). How did the late 1980s climate regime shift affect temperature-sensitive fish population dynamics: case study of vendace (Coregonus albula) in a large north-temperate lake. *Water*, *12*(10), 2694. DOI: https://doi.org/10.3390/w12102694

Kranenburg, W., Tiessen, M., Veenstra, J., de Graaff, R., Uittenbogaard, R., Bouffard, D., Sakindi, G., Umutoni, A., Van de Walle, J., Thiery, E., & van Lipzig, N. (2020). 3D-modelling of Lake Kivu: horizontal and vertical flow and temperature structure under spatially variable atmospheric forcing. *Journal of Great Lakes Research*, *46*(4), 947-960. DOI: 10.1016/j.jglr.2020.05.012

Kristensen, M. L., Righton, D., del Villar-Guerra, D., Baktoft, H., & Aarestrup, K. (2018). Temperature and depth preferences of adult sea trout Salmo trutta during the marine

migration phase. *Marine Ecology Progress Series*, *599*, 209-224. DOI: https://doi.org/10.3354/meps12618

Magnuson, J. J., Robertson, D. M., Benson, B. J., Wynne, R. H., Livingstone, D. M., Arai, T., Assel, R. A., Barry, R. G., Card, V., Granin, N. G., Prowse, D. T., Stewart, K.M. & Vuglinski, V. S. (2000). Historical trends in lake and river ice cover in the Northern Hemisphere. *Science, 289*(5485), 1743–1746. DOI: 10.1126/science.289.5485.1743

McDonald, C. P., Saeed, M. N., Robertson, D. M., & Prellwitz, S. (2022). Temperature explains the formation of a metalimnetic oxygen minimum in a deep mesotrophic lake. *Inland Waters, 12*(3), 331-340. DOI: https://doi.org/10.1080/20442041.2022.2029318

Menten, G., Melo, W., Pinho, J., Iglesias, I., & Antunes do Carmo, J. (2023). Simulation of Saltwater Intrusion in the Minho River Estuary under Sea Level Rise Scenarios. *Water*, *15*(13), 2313. DOI: 10.3390/w15132313

Mortimer, C. H., (1952). Water movements in lakes during summer stratification; evidence from the distribution of temperature in Windermere. *Philosophical Transactions of the Royal Society of London. Series B, Biological Sciences, 236*(635), 355-398. DOI: https://doi.org/10.1098/rstb.1952.0005

Muñoz Sabater, J. (2019): ERA5-Land hourly data from 1950 to present. Copernicus Climate Change Service (C3S) Climate Data Store (CDS). DOI: 10.24381/cds.e2161bac

NOAA CoastWatch Great Lakes Node: National Oceanic and Atmospheric Administration. (n.d.). *Lake surface temperature - CoastWatch Great Lakes Node*. NOAA. Retrieved March 19, 2025, from Lake Surface Temperature - Coastwatch Great Lakes Node

OpenMP Architecture Review Board. (2023). OpenMP application programming interface *version 5.2.* Retrieved from https://www.openmp.org/

Piccolroaz, S., Zhu, S., Ladwig, R., Carrea, L., Oliver, S., Piotrowski, A. P., Ptak, M., Shinohara, R., Sojka, M., Woolway, R. I., & Zhu, D. Z. (2024). Lake water temperature modeling in an era of climate change: Data sources, models, and future prospects. *Reviews of Geophysics*, *62*(1), e2023RG000816. DOI: https://doi.org/10.1029/2023RG000816

Régnier, T., Gibb, F. M., & Wright, P. J. (2017). Importance of trophic mismatch in a winter-hatching species: evidence from lesser sandeel. *Marine Ecology Progress Series, 567*, 185-197. DOI: https://doi.org/10.3354/meps12061

Rogers, K. B., & White, G. C. (2007). Analysis of movement and habitat use from telemetry data. *Analysis and interpretation of freshwater fisheries data. American Fisheries Society, Bethesda, Maryland*, 625-676. ISBN: 978-1-888569-77-3

Råman Vinnå, L., Wüest, A., & Bouffard, D. (2017). Physical effects of thermal pollution in lakes. *Water Resources Research*, *53*(5), 3968-3987. DOI: https://doi.org/10.1002/2016WR019686

SCB Statistics Sweden. *Kust, strander, öar.* (2008) Retrieved 2025-03-24 from https://web.archive.org/web/20100114041618/http://www.scb.se/Pages/TableAndChart____21205.aspx

Scheffer, M., & Carpenter, S. R. (2003). Catastrophic regime shifts in ecosystems: linking theory to observation. *Trends in ecology & evolution*, *18*(12), 648-656. DOI: https://doi.org/10.1016/j.tree.2003.09.002

Schmid, M., & Köster, O. (2016). Excess warming of a C entral E uropean lake driven by solar brightening. *Water Resources Research*, *52*(10), 8103-8116. DOI: https://doi.org/10.1002/2016WR018651

Schneider, P., & Hook, S. J. (2010). Space observations of inland water bodies show rapid surface warming since 1985. *Geophysical Research Letters, 37*(22). DOI: https://doi.org/10.1029/2010GL045059

Schwindt, S., Callau Medrano, S., Mouris, K., Beckers, F., Haun, S., Nowak, W., Wieprecht, S. & Oladyshkin, S. (2023). Bayesian calibration points to misconceptions in three-dimensional hydrodynamic reservoir modelling. *Water Resources Research*, *59*(3). DOI: 10.1029/2022WR033660

Sharaf, N., Lemaire, B. J., Fadel, A., Slim, K., & Vinçon-Leite, B. (2021). Assessing the thermal regime of poorly monitored reservoirs with a combined satellite and three-dimensional modeling approach. *Inland Waters*, *11*(3), 302-314. DOI: 10.1080/20442041.2021.1913937

Sharma, S., Gray, D. K., Read, J. S., O'reilly, C. M., Schneider, P., Qudrat, A., Gries, C., Stefanoff, S., Hampton, E. S., Hook, S., Lenters, D. J., Livingstone, D. M., McIntyre, P. B., Adrian, R., Allan, M. G., Anneville, O., Avola, L., Austin, J., Bailey, J., Baron, J. S., Brookes, J., Chen, Y., Daly, R., Dokulil, M., & Woo, K. H. (2015). A global database of lake surface temperatures collected by in situ and satellite methods from 1985–2009. *Scientific data*, *2*(1), 1-19. DOI: https://doi.org/10.1038/sdata.2015.8

SimScale. (2024). *CFL Condition in Computational Fluid Dynamics (CFD).* Retrieved 2025-05-08 from https://www.simscale.com/blog/cfl-condition/

SMHI. (n.d.-a). *Fakta om Vättern*. Retrieved 2025-03-21 from https://www.smhi.se/kunskapsbanken/hydrologi/de-stora-sjoarna/fakta-om-vattern

SMHI. (n.d.-b). *Vattentemperatur i sjöar*. Retrieved 2025-03-21 from https://www.smhi.se/kunskapsbanken/hydrologi/sveriges-sjoar/vattentemperatur-i-sjoar

Soulignac, F., Danis, P. A., Bouffard, D., Chanudet, V., Dambrine, E., Guénand, Y., Harmek, T., Ibelings, B-W., Trevisan, D., Uittenbogaard, R. & Anneville, O. (2018). Using 3D modeling and remote sensing capabilities for a better understanding of spatio-temporal heterogeneities of phytoplankton abundance in large lakes. *Journal of Great Lakes Research*, *44*(4), 756-764. DOI: 10.1016/j.jglr.2018.05.008

Steinmoeller, D. (2014). *High-order numerical methods in lake modelling*. (Phd thesis, University of Waterloo). Waterloo, Ontario, Canada: University of Waterloo

Swedish University of Agricultural Sciences. (n.d.). *SLU Geodata Catalog*. Retrieved 2025-03-25 from https://www.slu.se/site/bibliotek/soka-och-lana/soka/digitala-kartor/

Swedish University of Agricultural Sciences (SLU). *Rödingen i Vättern spåras i nytt projekt*. 2021. Retrieved 2025-03-20 from https://internt.slu.se/nyheter-originalen/2021/8/rodingen-i-vattern-sparas-i-nytt-projekt/

Thorstad, E. B., Rikardsen, A. H., Alp, A., & Økland, F. (2013). The use of electronic tags in fish research–an overview of fish telemetry methods. *Turkish Journal of Fisheries and Aquatic Sciences*, *13*(5), 881-896. DOI: 10.4194/1303-2712-v13_5_13

Upreti, H., & Ojha, C. S. P. (2017). Estimation of relative humidity and dew point temperature using limited meteorological data. *Journal of irrigation and drainage engineering*, *143*(9), 05017005. DOI: https://doi.org/10.1061/(ASCE)IR.1943-4774.0001225

Venäläinen, A., Frech, M., Heikinheimo, M., & Grelle, A. (1999). Comparison of latent and sensible heat fluxes over boreal lakes with concurrent fluxes over a forest: implications for regional averaging. *Agricultural and forest meteorology*, *98*, 535-546. DOI: https://doi.org/10.1016/S0168-1923(99)00100-8

Vätternvårdsförbundet. *Vätterns tillstånd idag.* (n.d.) Retrieved 2025-03-24 from: https://vattern.org/om-vattern/vatterns-tillstand-idag/

Whitehead, P. G., Wilby, R. L., Battarbee, R. W., Kernan, M., & Wade, A. J. (2009). A review of the potential impacts of climate change on surface water quality. *Hydrological sciences journal*, *54*(1), 101-123. DOI: https://doi.org/10.1623/hysj.54.1.101

Williams, J. J., & Esteves, L. S. (2017). Guidance on setup, calibration, and validation of hydrodynamic, wave, and sediment models for shelf seas and estuaries. *Advances in civil engineering*, *2017*(1), 5251902. DOI: https://doi.org/10.1155/2017/5251902
Yang, K., Yu, Z., & Luo, Y. (2020). Analysis on driving factors of lake surface water temperature for major lakes in Yunnan-Guizhou Plateau. *Water Research*, *184*, 116018. DOI: https://doi.org/10.1016/j.watres.2020.116018

Appendices

Appendix 1

As part of a master's thesis, a Delft3D model was configured to simulate hourly three-dimensional water temperatures in Lake Vättern, Sweden, throughout the year 2023. The following appendix provides an overview of the parameters used for the model setup, along with references supporting the selection of each parameter value.

The simulation timestep was initially guided by the approach used by Amadori et al. (2021) and was later validated using the Courant-Friedrichs-Lewy (CFL) condition, as described in a later section of the methodology. The CFL criterion was set to a maximum value of 0.6, following descriptions from the Delft3D technical reference documentation (Deltares 2024). Wind drag coefficients were parameterized as a linear function of wind speed, ranging from 6.3×10^{-4} at 0 m/s to 7.23×10^{-3} at 100 m/s, in accordance with the Delft3D manual (Deltares 2024). Additionally, the Heat Flux Model (Composite) and the Turbulence Model (k-ε) were selected based on their applicability, as outlined in the Delft3D manual (Deltares 2024).

Boundary conditions for the model were set to Partial Slip, reflecting the shoreline characteristics of Lake Vättern, which consisted of a combination of vertical rock walls and more gently sloping shore zones (Vätternvårdsförbundet, n.d.). Bottom roughness was specified using the Chezy coefficient value 60 $m^{1/2}s^{-1}$, as employed by Amadori et al. (2021). Sensitivity tests conducted within that study indicated that variations in this parameter had negligible impact on model results, confirming its suitability as a commonly adopted roughness coefficient.

Secchi depth measurements, conducted by the Swedish County Board during previous studies, indicate a water transparency of 10 meters (F. Ermold, personal communication, April 10, 2025). Horizontal eddy viscosity and horizontal eddy diffusivity were maintained at default values, consistent with the approach of Amadori et al. (2021). Additionally, these parameters were not identified as highly sensitive in the sensitivity analysis by Chanudet et al. (2012). The initial temperature conditions were derived from the processed telemetry data, indicating a uniform temperature across the entire lake of 5°C at the start of the simulation. For parameters identified by Chanudet et al. (2012) as exerting a significant influence on simulation output, the same values as those used by Amadori et al. (2021) were implemented. Specifically, the Stanton number was set to 6.5×10^{-4}, the Dalton number to 1.3×10^{-3}, and the free convection coefficient to 1.0×10^{-1}. The background vertical eddy viscosity and diffusivity were set to zero, reflecting their role as minimum values within the simulation framework. This approach ensures that the physical minimum is utilized, preventing artificial mixing effects (Amadori et al., 2021).

Table S1: A Delft3D Flexible Mesh Suite model was developed for Lake Vättern, Sweden. In this study the model was three-dimensional and simulated hourly lake water temperatures from January 1st, 2023, to December 31st, 2023. The table presents the model settings and parameters used, along with references to justify the selected values. The sensitive parameters listed at the end of the table have been described in the literature as having a significant influence on model output. These parameter values were chosen based on studies of a lake with physical characteristics similar to those of Lake Vättern.

Model setting	**Value**	**Reference**
Simulation time step	60 s	Amadori et al. (2021)
Max Courant-Friedrichs-Lewy	0.6	Deltares (2024)
Horizontal grid spacing	200-950 m	
Vertical grid spacing	1-1.8 m	Sigma growth factor
Wind drag coefficients	6.3×10^{-4} 7.23×10^{-3}	Deltares (2024)
Wall boundary conditions	Free slip	Vätternvårdsförbundet, (n.d.)
Heat flux model	Composite	Deltares (2024)
Turbulence model	k-ε	Deltares (2024)
Secchi depth	10 m	Swedish County Board (2025)
Bottom roughness	Chezy 60 $m^{1/2}s^{-1}$	Amadori et al. (2021)
Horizontal eddy viscosity	2×10^{-1} m^2s^{-1}	Amadori et al. (2021)
Horizontal eddy diffusivity	2×10^{-1} m^2s^{-1}	Amadori et al. (2021)
Initial temperature	5 C°	Telemetry data
Sensitive parameters (Chanudet et al., 2012)		
Stanton number	6.5×10^{-4}	Amadori et al. (2021)
Dalton number	1.3×10^{-3}	Amadori et al. (2021)
Free convection coefficient	1.0×10^{-1}	Amadori et al. (2021)
Background vertical eddy viscosity	0 m^2s^{-1}	Amadori et al. (2021)
Background vertical eddy diffusivity	0 m^2s^{-1}	Amadori et al. (2021)

References

Amadori, M., Giovannini, L., Toffolon, M., Piccolroaz, S., Zardi, D., Bresciani, M., Giardion, C., Luciani, G., Kliphuis, M., Haren, H. & Dijkstra, H. A. (2021). Multi-scale evaluation of a 3D lake model forced by an atmospheric model against standard monitoring data. *Environmental Modelling & Software*, *139*, 105017. https://doi.org/10.1016/j.envsoft.2021.105017

Chanudet, V., Fabre, V., & van der Kaaij, T. (2012). Application of a three-dimensional hydrodynamic model to the Nam Theun 2 Reservoir (Lao PDR). *Journal of Great Lakes Research*, *38*(2), 260-269. DOI: 10.1016/j.jglr.2012.01.008

Deltares. (2024). *D-Flow Flexible Mesh: Technical Reference Manual* (Version 2025, Revision 79761). Deltares systems.

Vätternvårdsförbundet. *Vätterns tillstånd idag.* (n.d.) Retrieved 2025-03-24 from: https://vattern.org/om-vattern/vatterns-tillstand-idag/